Chapter 5

RESULTS & DISCUSSION

5.1 HPLC analytical method development and validation in PBS (pH 5.5) and plasma

5.1.1 Range and Linearity

The calibration curves for GEM and EGCG in PBS (pH 5.5) and plasma are shown in the figure. A linear relationship was observed between the concentrations of GEM at 268 nm and EGCG at 280 nm in both PBS (pH 5.5) and plasma, and their chromatographic area under the curve. The table 5 presents the correlation coefficient and slope of all calibration curves. The high correlation coefficient values for calibration curves of GEM and EGCG in in-vitro and in-vivo samples of the fitted model demonstrate a robust relationship among the variables. This strong correlation confirms the model's suitability for further analysis and application.

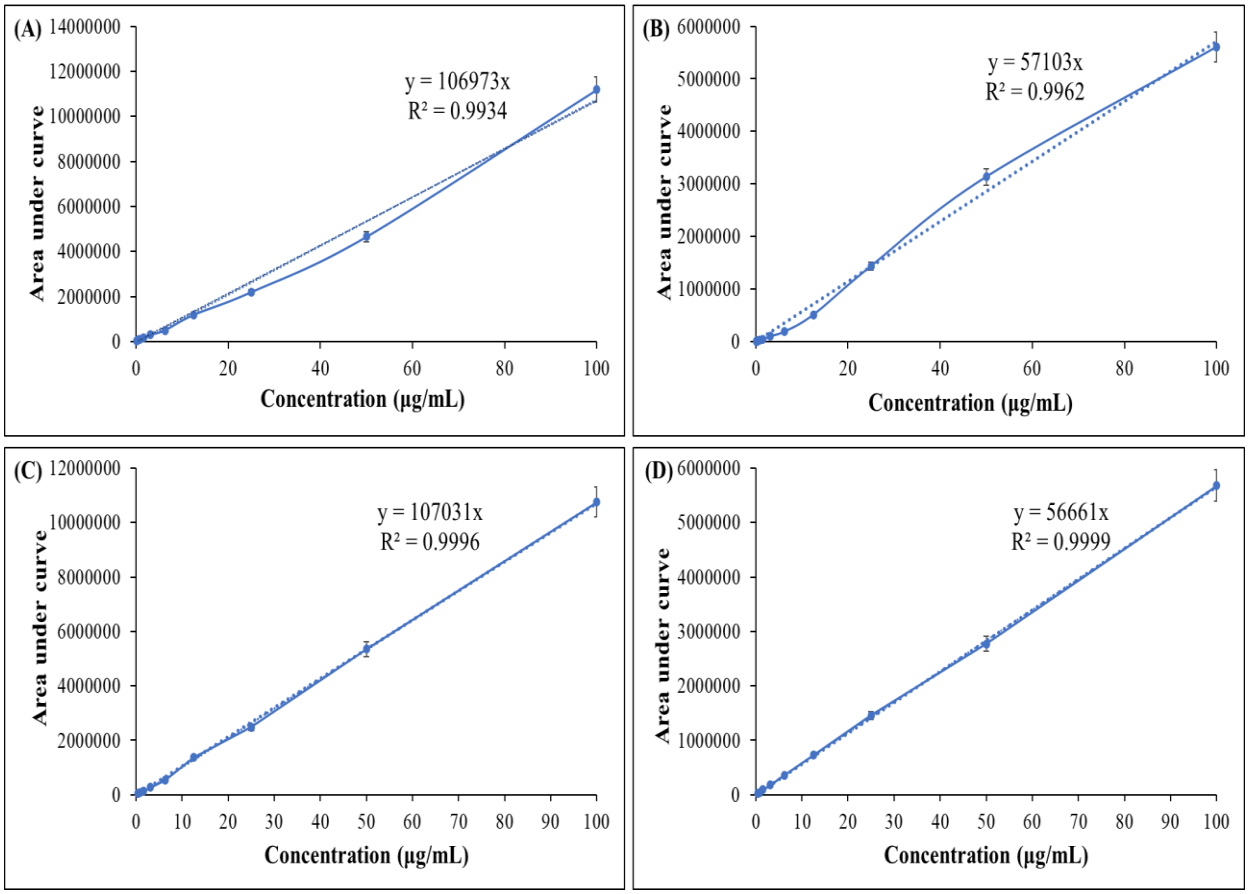

Figure 7: Calibration curves of (A) GEM in PBS (pH 5.5) at wavelength 268 nm; (B) EGCG in PBS (pH 5.5) at wavelength 280 nm; (C) GEM in plasma at wavelength 268 nm; and (D) EGCG in plasma at wavelength 280 nm.

Table 5: HPLC validation parameters for determination of GEM and EGCG in PBS (pH 5.5) and plasma (the data has been presented as mean ± SD (n=3))

Parameters	pH 5.5		Plasma	
	GEM	**EGCG**	**GEM**	**EGCG**
Wavelength (nm)	268	280	268	280
Retention time (min)	6	8	6	8
Slope	106973	57103	107031	56661
Correlation coefficient (R^2)	0.9934	0.9962	0.9996	0.9999
Range (µg/mL)	0.097 – 100	0.097 – 100	0.390 – 100	0.390 – 100
LOD (ug/ml)	104.81	104.19	111.03	109.96
LOQ (ug/ml)	317.61	315.74	336.46	333.23

5.1.2 Accuracy and precision

The analytical HPLC method's accuracy is shown by the closeness between theoretical (added concentrations) and experimental (recovered concentrations) values. Precision refers to the consistency of readings from multiple samplings of the same homogeneous sample under specific analytical conditions. This is determined by analyzing standard samples at three different concentrations in triplicate within the calibration range.

The method's accuracy, expressed as the percentage of drug recovered, was found to be between 98% and 102% for GEM and EGCG, indicating that the method is within the acceptable limits. The intraday and interday precision, represented by the relative standard

deviation value, was found to be less than 2%, demonstrating the repeatability of the developed HPLC method (table 6).

Table 6: Accuracy & precision (Intra-day and inter-day precision) studies of the developed analytical HPLC method for GEM and EGCG in PBS (pH 5.5) and plasma

Samples	Standard sample (µg/mL)	Level of recovery	Drug added (µg/mL)	Drug recovered (µg/mL) (mean±SD)	Percent drug recovered	Precision	
						Intraday	Interday
pH 5.5 (GEM)	100	80 %	80	81.25±0.23	101.56	1.12	1.58
		100 %	100	99.10±0.57	99.10	1.43	1.94
		120 %	120	120.00±0.32	100.00	1.79	1.55
pH 5.5 (EGCG)	100	80 %	80	79.10±0.29	98.86	1.21	1.01
		100 %	100	102.92±0.45	102.92	1.97	1.44
		120 %	120	119.00±0.51	99.17	1.95	1.96
Plasma (GEM)	100	80 %	80	79.72±0.14	99.65	1.42	1.93
		100 %	100	99.01±0.38	99.01	1.73	1.77
		120 %	120	118.00±0.29	98.33	1.85	1.92
Plasma (EGCG)	100	80 %	80	78.92±0.41	98.65	1.41	1.38
		100 %	100	99.50±0.18	99.50	1.62	1.25
		120 %	120	119.01±0.35	99.18	1.29	1.94

5.1.3 Specificity, selectivity and sensitivity

The developed method demonstrated strong specificity and selectivity, with no interfering peaks (figure) observed at the retention time of GEM and EGCG, indicating clear specificity. For sensitivity assessment, **the limit of detection** (**LOD**) and **limit of quantitation** (**LOQ**) were calculated. LOD indicates the minimum analyte concentration detectable, though not necessarily precisely quantifiable. LOQ refers to the minimum analyte concentration that can

be accurately and precisely quantified. The determination of LOD and LOQ followed established protocols and specific equations as outlined in ICHQ2 (R1).

LOD = 3.3 SD/Slope **Eq. 7**

LOQ = 10 SD/Slope **Eq. 8**

The LOD and LOQ values for GEM and EGCG in PBS (pH 5.5) (Table 3.3) were 104.81 (GEM), 104.19 (EGCG), 317.61 (GEM), and 315.74 (EGCG), respectively. For plasma samples, the LOD and LOQ values were 111.03 (GEM), 109.96 (EGCG), 333.46 (GEM), and 333.23 (EGCG), respectively. These lower LOD and LOQ values highlight the sensitivity of the developed HPLC method for detecting GEM and EGCG. Calibration curves were prepared from the LOQ onwards during analysis.

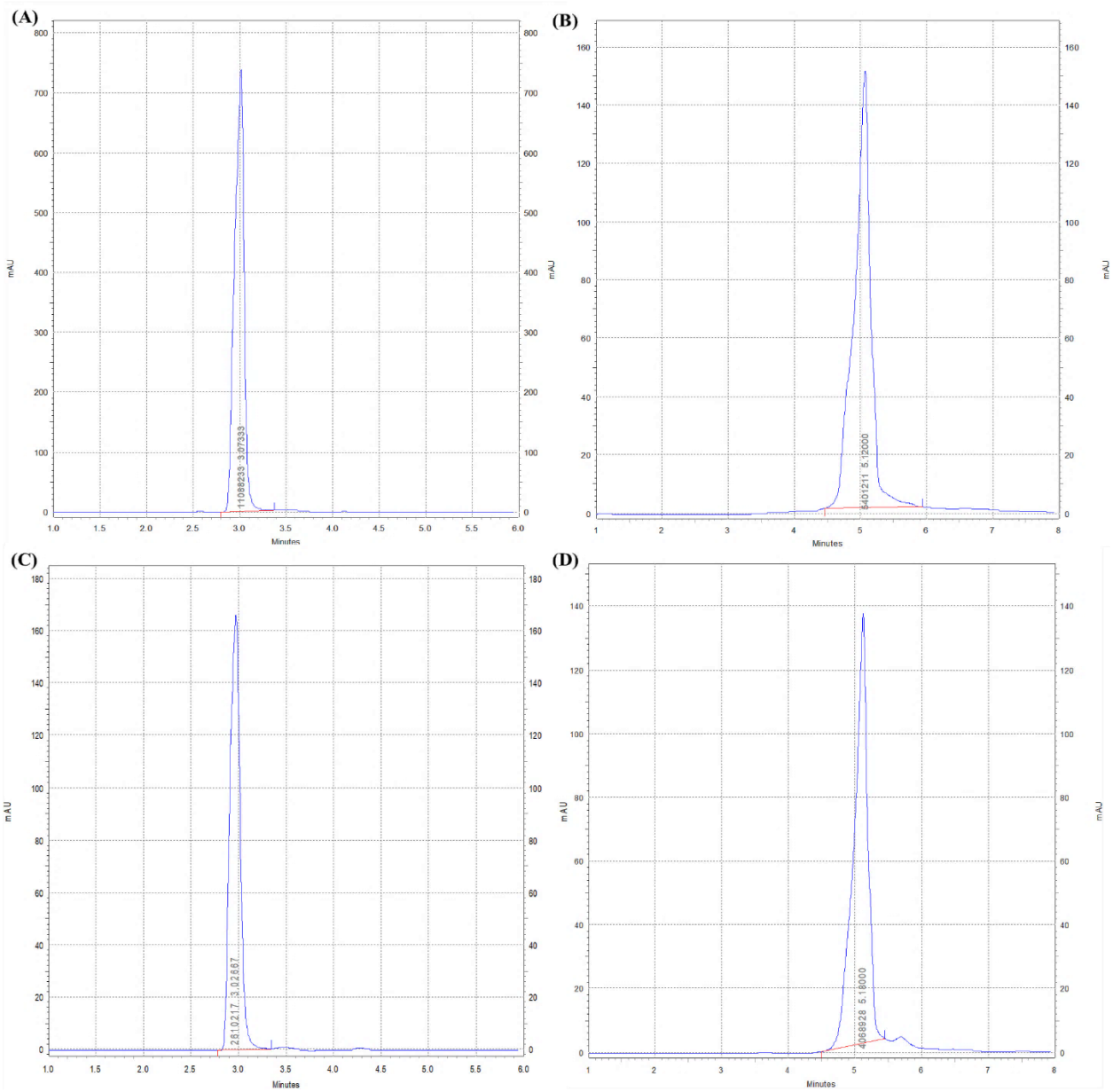

Figure 8: Selectivity of (A) GEM in PBS (pH 5.5) at wavelength 268 nm; (B) EGCG in PBS (pH 5.5) at wavelength 280 nm; (C) GEM in plasma at wavelength 268 nm; and (D) EGCG in plasma at wavelength 280 nm.

5.2 Optimization studies

A 2-level 3-factor factorial design model was fitted and analyzed for all four responses. It can be inferred from the ANOVA (table 8) and FIT (suggesting goodness of fit) statistics (table 9)

tables, that the model is significant for all four responses. The significance of a model is described in terms of Fischer test value (F-value) and probability values (p-value) in ANOVA, the higher the F-value and the lower the p-value (< 0.05), the significance of the model is likely to be more. The model F-value for particle size is 62.47 and $p < 0.05$ which depicts a significant model for the response studied. Similarly, for PDI the observed model F-value corresponds to 49.18 and the p-value is 0.0013 (less than 0.05) which is again in accordance with the significant model for the response. The model F-value for entrapment efficiency of GEM (51.66) and EGCG (13.44) is also in tune with the significant model and the p-value is lower than 0.05 for both the responses. The table for FIT statistics portrays well that the values of predicted R^2 are in accordance with the adjusted R^2 values and the values of adeq precision are higher than 4 for all four responses, which is desirable for the validation of the model. The value of adeq precision calculates the ratio between signal and noise which is agreeable if reported to be higher than 4 and substantiates that the model can be employed to navigate the design space.

Table 7: Independent factors considered during the optimization of the formulation along with the responses studied.

	Factor 1	**Factor 2**	**Factor 3**	**Response 1**	**Response 2**	**Response 3**	**Response 4**
Run	A: Lipid	B: Surfactant	C: Phospholipid	Particle size	PDI	Entrapment efficiency of GEM	Entrapment efficiency of EGCG
	mg	%	mg	nm		%	%
1	-1	-1	-1	147.72	0.332	93.390	77.903
2	1	1	1	123.9	0.117	92.343	89.490
3	-1	1	1	135.54	0.119	95.060	94.790
4	1	-1	-1	148.79	0.337	90.308	77.860

5	-1	-1	1	127.4	0.202	94.960	87.850
6	1	1	-1	142.4	0.256	89.980	78.450
7	1	-1	1	132.7	0.250	93.330	85.000
8	-1	1	-1	135.4	0.257	92.830	77.480

Table 8: Statistical analysis (ANOVA) table for all the selected responses of the factorial model.

Response	**Source**	**Sum of Squares**	**df**	**Mean Square**	**F-value**	**p-value**	
Particle size	**Model**	963.39	3	321.13	62.47	0.0008	Significant
PDI	**Model**	0.0481	3	0.0160	49.18	0.0013	Significant
Entrapment efficiency of GEM	**Model**	24.15	3	8.05	51.69	0.0012	Significant
Entrapment efficiency of EGCG	**Model**	281.40	3	93.80	13.44	0.0148	Significant

* df corresponds to degrees of freedom

Table 9: FIT statistics table for all the responses studied.

Response	**Std. Dev.**	**Mean**	**C.V. %**	**R^2**	**Adjusted R^2**	**Predicted R^2**	**Adeq Precision**
Particle size	2.27	131.73	1.40	0.9791	0.9634	0.9164	21.1866
PDI	0.0181	0.2337	7.73	0.9736	0.9538	0.8944	17.9332
Entrapment	0.3946	92.78	0.4253	0.9749	0.9560	0.8994	19.0291

efficiency of GEM							
Entrapment efficiency of EGCG	2.64	83.60	3.16	0.9098	0.8421	0.6390	8.6001

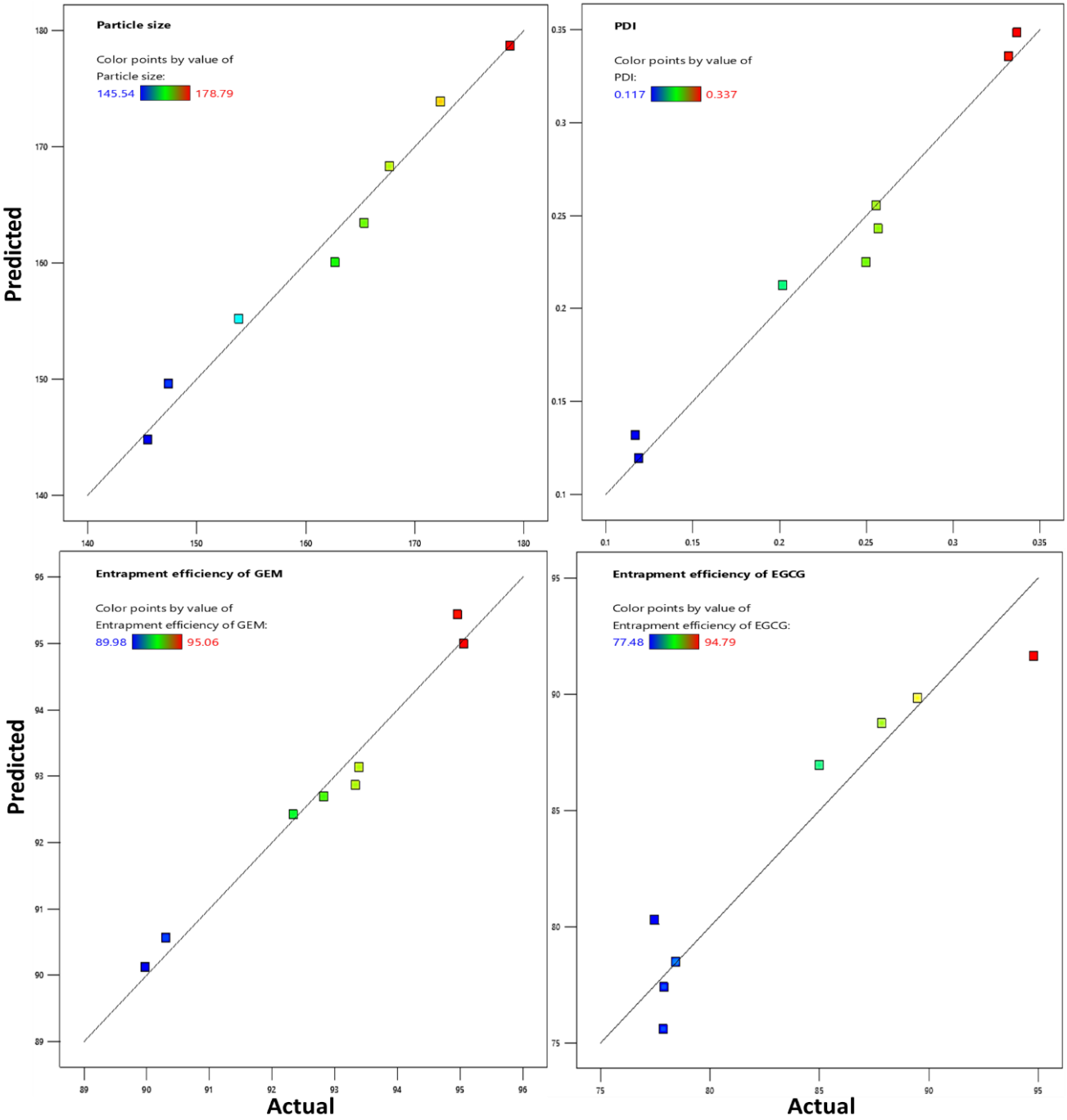

Figure 9: Predicted vs. actual graph for all the four responses viz., particle size, PDI, entrapment efficiency of GEM, and entrapment efficiency of EGCG.

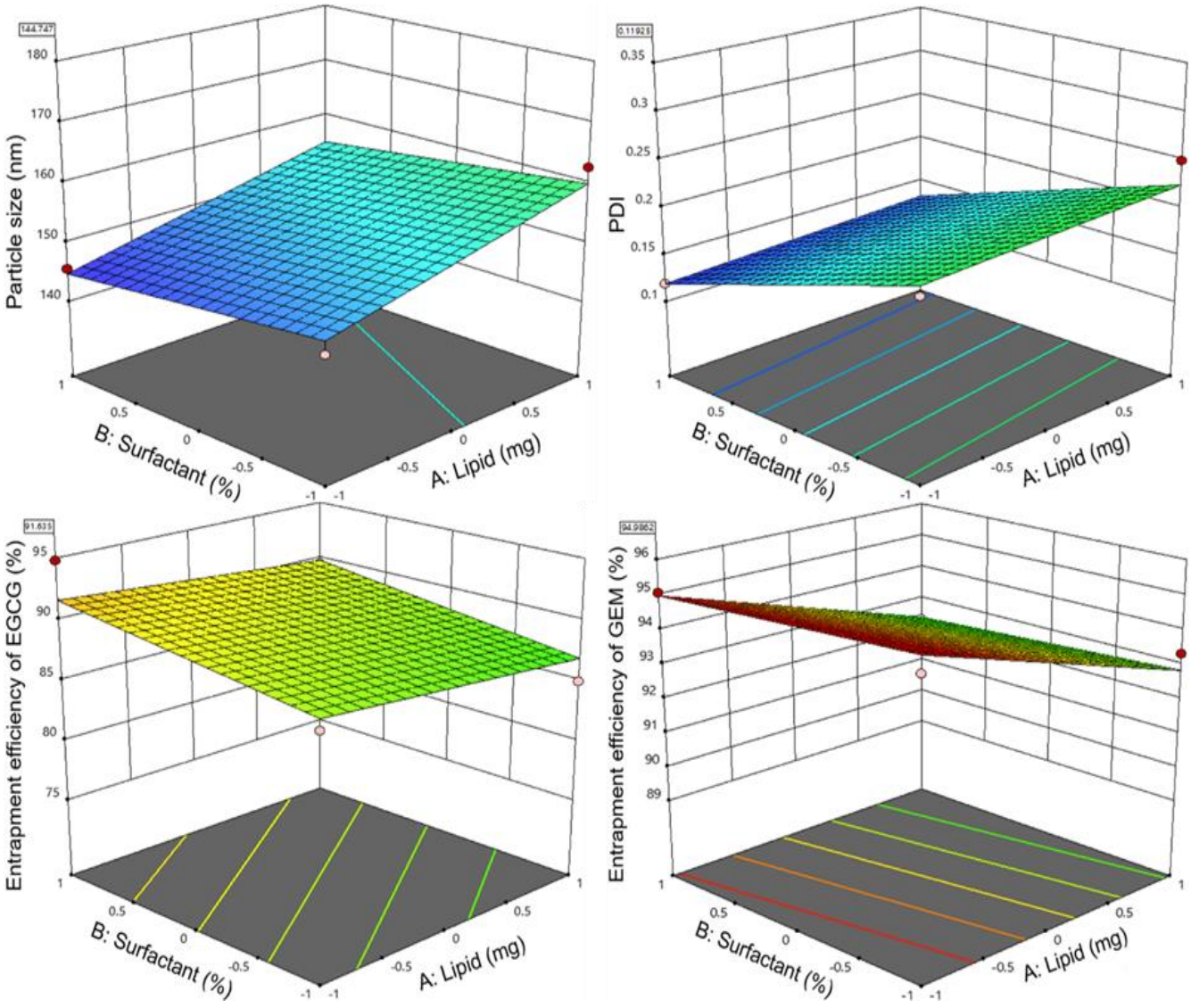

Figure 10: 3-D Contour plots for the responses viz., particle size, PDI, entrapment efficiency of GEM, and entrapment efficiency of EGCG.

Validation of the model, suggested 100 solutions (table 8), from which solution number 6 was opted for our protocol.

Table 10: The solutions predicted by the model upon validation.

S.No.	Lipid	Surfactant	Phospholipid	Particle size (nm)	PDI	Entrapment efficiency of GEM (%)	Entrapment efficiency of EGCG (%)	Desirability
1	0.156	0.944	0.367	126.829	0.168	92.787	86.915	1.000
2	1.000	1.000	-1.000	143.873	0.255	90.120	78.470	1.000
3	-1.000	1.000	-1.000	133.440	0.243	92.690	80.276	1.000
4	1.000	1.000	1.000	125.180	0.132	92.416	89.829	1.000
5	-1.000	-1.000	-1.000	138.282	0.336	93.134	77.376	1.000
6	**1.000**	**-1.000**	**1.000**	**120.748**	**0.119**	**94.986**	**91.635**	**1.000**
7	1.000	-1.000	-1.000	148.715	0.348	90.564	75.571	1.000
8	-1.000	-1.000	1.000	129.590	0.212	95.430	88.736	1.000
9	-0.824	0.950	0.617	129.367	0.146	94.331	89.228	1.000
10	0.443	-0.830	-0.040	136.427	0.278	92.344	81.771	1.000
11	0.239	0.366	-1.000	141.437	0.280	91.239	78.238	1.000
12	0.003	-0.363	-0.119	123.737	0.258	92.715	82.398	1.000
13	-0.774	-0.727	-0.361	132.828	0.285	93.516	81.198	1.000
14	-0.721	0.271	0.930	128.624	0.159	94.709	89.927	1.000
15	0.536	-0.126	0.063	134.237	0.239	92.187	83.298	1.000
16	-0.099	0.201	0.646	124.690	0.184	93.599	87.652	1.000
17	0.031	0.007	-0.708	138.496	0.277	91.921	79.563	1.000
18	-0.972	-0.355	0.279	124.915	0.227	94.423	85.550	1.000
19	-0.245	-0.071	0.660	124.451	0.195	93.864	87.472	1.000
20	-0.304	-0.971	0.067	131.864	0.273	93.459	82.853	1.000
21	-0.632	0.969	-0.278	128.692	0.202	93.052	83.997	1.000

22	-0.689	0.338	0.516	122.498	0.182	94.177	87.646	1.000
23	-0.976	0.872	-0.643	130.541	0.227	93.097	82.095	1.000
24	-0.323	-0.253	-0.296	133.425	0.262	92.906	81.848	1.000
25	-0.865	-0.085	0.271	124.891	0.216	94.217	85.800	1.000
26	-0.537	0.224	0.978	129.249	0.160	94.538	89.967	1.000
27	0.745	-0.781	0.591	131.986	0.238	92.670	85.154	1.000
28	-0.239	-0.793	0.064	121.805	0.265	93.332	83.033	1.000
29	-0.866	0.401	-0.062	126.824	0.214	93.727	84.614	1.000
30	0.550	0.902	0.484	127.892	0.165	92.424	87.163	1.000
31	0.629	-0.528	0.641	130.298	0.223	92.820	85.912	1.000
32	0.878	0.307	-0.213	137.556	0.238	91.335	82.046	1.000
33	-0.350	-0.666	-0.164	133.050	0.273	93.184	82.023	1.000
34	-0.964	0.150	-0.117	127.431	0.228	93.846	84.028	1.000
35	0.129	-0.519	0.971	124.586	0.199	93.839	88.249	1.000
36	-0.546	0.766	-0.260	129.456	0.211	93.009	83.730	1.000
37	0.930	0.799	-0.110	135.678	0.209	91.276	83.295	1.000
38	-0.635	-0.733	-0.217	132.226	0.277	93.504	81.879	1.000
39	-0.933	-0.381	0.659	121.627	0.205	94.815	87.635	1.000
40	-0.789	-0.943	-0.205	131.814	0.285	93.763	81.784	1.000
41	0.877	-0.872	0.883	130.170	0.225	92.855	86.560	1.000
42	-0.513	0.886	-0.210	128.870	0.202	92.997	84.159	1.000
43	0.323	0.730	0.760	124.543	0.155	93.071	88.687	1.000
44	0.114	0.630	0.411	126.965	0.180	92.960	86.744	1.000
45	0.097	-0.652	0.034	133.497	0.263	92.835	82.764	1.000
46	0.326	0.056	0.008	133.221	0.233	92.353	83.435	1.000

47	-0.236	0.191	-0.310	132.938	0.243	92.679	82.331	1.000
48	0.961	0.467	-0.810	143.188	0.268	90.506	78.810	1.000
49	0.281	0.254	-0.806	140.116	0.273	91.432	79.140	1.000
50	0.035	-0.232	-0.277	135.071	0.262	92.463	81.659	1.000
51	0.571	-0.265	-0.843	143.235	0.302	91.131	77.914	1.000
52	-0.448	-0.986	-0.784	139.115	0.325	92.668	78.122	1.000
53	-0.565	-0.644	0.778	123.068	0.212	94.538	87.600	1.000
54	0.650	0.739	-0.486	137.877	0.233	91.218	81.325	1.000
55	-0.525	0.839	0.613	121.229	0.154	93.968	88.776	1.000
56	-0.659	-0.582	-0.440	133.821	0.284	93.245	80.852	1.000
57	-0.352	0.711	-0.441	132.295	0.226	92.563	82.447	1.000
58	-0.433	-0.479	-0.297	133.413	0.272	93.096	81.610	1.000
59	0.895	-0.299	-0.397	140.839	0.278	91.235	80.104	1.000
60	0.858	0.371	0.579	129.899	0.186	92.255	86.654	1.000
61	0.546	-0.119	-0.158	136.343	0.252	91.919	82.041	1.000
62	0.170	-0.823	0.357	131.270	0.251	93.150	84.286	1.000
63	0.670	-0.280	0.888	127.607	0.196	92.996	87.634	1.000
64	-0.290	0.020	0.173	128.546	0.220	93.343	84.880	1.000
65	-0.044	-0.910	0.039	133.338	0.273	93.078	82.546	1.000
66	-0.661	-0.370	-0.941	137.977	0.305	92.626	78.317	1.000
67	-0.657	-0.569	0.058	129.142	0.253	93.812	83.699	1.000
68	-0.711	-0.185	0.867	120.367	0.184	94.725	88.902	1.000
69	-0.353	0.471	-0.940	137.535	0.268	92.045	79.265	1.000
70	-0.965	-0.434	0.215	125.740	0.235	94.358	85.066	1.000
71	0.646	0.666	-0.120	134.614	0.214	91.659	83.302	1.000

72	0.739	0.191	-0.802	142.620	0.279	90.862	78.658	1.000
73	0.187	0.621	0.418	127.295	0.180	92.877	86.709	1.000
74	-0.436	0.085	0.591	123.735	0.191	93.994	87.473	1.000
75	0.798	0.110	0.990	126.377	0.173	92.862	88.664	1.000
76	-0.054	-0.325	0.055	131.729	0.245	92.979	83.489	1.000
77	0.521	-0.793	0.724	129.601	0.229	93.113	86.097	1.000
78	-0.171	0.752	0.601	123.406	0.161	93.517	88.259	1.000
79	0.891	-0.087	-0.737	143.479	0.289	90.803	78.486	1.000
80	-0.750	0.040	-0.843	135.599	0.279	92.762	79.550	1.000
81	-0.699	-0.664	0.183	127.981	0.249	94.031	84.312	1.000
82	-0.341	0.687	0.580	122.874	0.164	93.726	88.198	1.000
83	0.587	-0.908	-0.526	141.907	0.312	91.618	78.770	1.000
84	-0.250	0.865	-0.296	131.102	0.210	92.564	83.401	1.000
85	0.185	0.436	-0.653	137.744	0.255	91.690	80.360	1.000
86	0.962	-0.930	-0.934	147.731	0.341	90.673	76.080	1.000
87	-0.012	-0.400	0.445	128.477	0.225	93.390	85.562	1.000
88	0.395	0.935	-0.921	140.131	0.250	91.003	79.373	1.000
89	0.384	-0.313	0.517	129.654	0.219	92.946	85.742	1.000
90	0.641	-0.395	0.166	134.475	0.246	92.230	83.397	1.000
91	0.407	0.927	-0.237	133.823	0.208	91.774	83.235	1.000
92	0.228	0.204	-0.863	140.493	0.279	91.446	78.792	1.000
93	0.128	0.305	-0.816	139.293	0.271	91.605	79.292	1.000
94	-0.198	0.036	0.704	124.031	0.187	93.830	87.832	1.000
95	-0.827	0.678	-0.252	128.128	0.213	93.399	83.902	1.000
96	-0.767	0.638	0.951	127.303	0.141	94.710	90.619	1.000

97	-0.968	0.287	0.290	123.277	0.196	94.288	86.540	1.000
98	0.740	0.842	-0.721	140.289	0.244	90.810	80.061	1.000
99	0.330	-0.779	-0.427	139.330	0.298	92.033	79.751	1.000
100	0.326	0.904	0.777	123.983	0.146	93.048	89.030	1.000

5.3 Characterization of SLNs

5.3.1 Micromeritics and zeta potential

QbD-optimized gemcitabine and epigallocatechin-3-gallate loaded solid lipid nanoparticles (GEM-EGCG SLNs) were prepared by the double emulsification solvent evaporation technique. The diagrammatic representation of GEM-EGCG SLNs is depicted in figure 9.

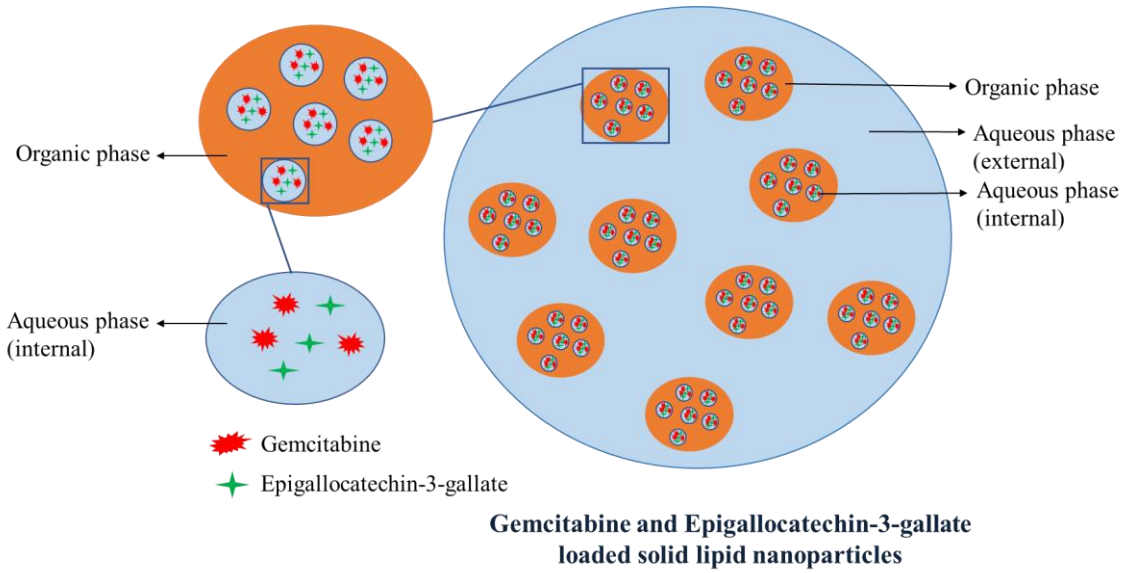

Figure 11: Diagrammatic representation of gemcitabine and epigallocatechin-3-gallate loaded solid lipid nanoparticles (GEM-EGCG SLNs).

The average particle size and PDI of SLNs was determined by Malvern Zetasizer Pro (Malvern, UK) at Biophysics & Nanotechnology Lab, Department of Physics, IIT BHU, Varanasi, India, based on dynamic light scattering phenomenon. The intranasal route of drug

administration is a means of drug delivery via the nose which has been used to treat conditions such as seasonal rhinitis during the last century [50]. Since the early twentieth century, the intranasal route of administration has been explored for treating systemic diseases, and conditions related to the lungs such as asthma [165], lung cancer, chronic obstructive pulmonary disease [165], respiratory distress syndrome, pulmonary fibrosis, and neurological disorders like Parkinson's disease, epilepsy, Alzheimer's disease, glioblastoma, and depression as well [50], [166]. Obvious merits that are offered by the intranasal route of drug administration include non-invasiveness, bypass of first-pass metabolism, lower dose as compared to the systemic route [166], increased bioavailability, can target lungs directly [167], ability to cross the blood-brain barrier, and the potential to control metastases [168] of lung cancer in the brain via trigeminal or olfactory nerve [50], [166], [167]. However, the challenges faced by the intranasal route of drug administration include formulation characteristics such as particle size, surface charge (zeta potential), shape, pH, biocompatibility, permeability, and retention [167], [169]. Particle size has a direct effect on lung deposition, the smaller the particle size (less than 10 μm [170]) better the penetration and deposition in the lungs [171], [172] whereas larger-sized particles are obstructed in the upper airways and are employed for the treatment of medical conditions of the upper respiratory region. It has been reported that particles having sizes in the range of 5 μm to 10 μm target the oropharyngeal region and large conducting airways [173] whereas particles with sizes of 1 μm to 5 μm are deposited in the alveolar region and small airways [174]. Particles with size of less than 3 μm have more than 80% chance of reaching lower respiratory regions with more than 60 % deposition in the alveoli [171], [175]. Particles having a size less than 1 μm are reported to have higher pulmonary distribution and reach into distal airways [172]. The average particle size of GEM-EGCG SLNs, GEM SLNs, and EGCG SLNs were found to be 122.8 ± 8.02 nm, 118.9 ± 12.71 nm, and 117.4 ± 9.37 nm, respectively, while PDI was found to be 0.1738 ± 0.02, 0.257

± 0.03, and 0.202 ± 0.05 for GEM-EGCG SLNs, GEM SLNs, and EGCG SLNs respectively. The average particle size of all three formulations is in the nanosize range with monodisperse particles which is desirable for our study. The 3-D contour plots (figure 10) for particle size depict a strong correlation between the amount of lipid and the percentage of surfactants on the average particle size. Increasing the amount of lipid will proportionally increase the average particle size which suggests that lipid demonstrates a positive effect on the average particle size of the SLNs formulation. This could be attributed to the enlargement of the lipidic layer and viscosity [176] with an increase in the amount of lipid during the formation of W/O primary emulsion which in turn results in the increase of the average particle size. Literature review indicates that slight variations in lipid composition significantly affects the quality of SLNs dispersion. Moreover, lipid content impacts the particle size of SLNs during high-shear homogenization. Typically, increasing lipid content above 5-10% leads to larger particles and a wider size distribution [177], [178], [179]. The type of surfactant and their concentration play a crucial role in determining the quality of SLNs. Both, individual surfactants or a mixture of surfactants influence the size of the lipid nanoparticles [179]. As per 3-D contour plots (figure 10) for particle size, an inverse relationship was observed between the percentage of surfactants and average particle size, such that an increase in the amount of surfactant may lead to decrease in average particle size of SLNs probably due to better emulsification and a decrease in interfacial tension [179], [180]. For any colloidal system, zeta potential values govern their electrostatic stability with values greater than ± 25.0 mV resulting in highly stable systems. Several studies have reported that zeta potential has a significant impact on drug retention in the nasal mucosa region. Mucin found in the nasal mucosa bears a negative charge [181], hence formulations with positive zeta potential value result in better electrostatic attraction and facilitate longer retention time and enhance attachment with nasal mucosa [46], [182], [183], [184]. The values for zeta potential of GEM-

EGCG SLNs, GEM SLNs, and EGCG SLNs were found to be -35.9 ± 1.6 mV, -33.9 ± 2.1 mV, and -24.0 ± 2.7 mV, respectively. The values of zeta potential correspond to higher particle stability of SLNs which is of course desirable for the long-term stability of the formulation. The negative zeta potential demonstrates repulsion between the negatively charged mucin in the nasal mucosa and GEM-EGCG SLNs and hence GEM-EGCG SLNs could have traversed into the respiratory region with ease in the absence of any electrostatic attraction or attachment [185]. The high value of zeta potential also reflects the stability of the GEM-EGCG SLNs [176]. The zeta potential can also influence the proficiency of particles to permeate across the biological membrane and toxicity associated with disruption of the cell wall [182], [183].

5.3.2 Surface morphology analysis

The surface morphology of GEM-EGCG SLNs was evaluated by scanning electron microscope (Zeiss Supra 40, Evo Research Ltd., Japan) [121]. SEM image (figure 12 (B)) shows that GEM-EGCG SLNs have uniform spherical morphology.

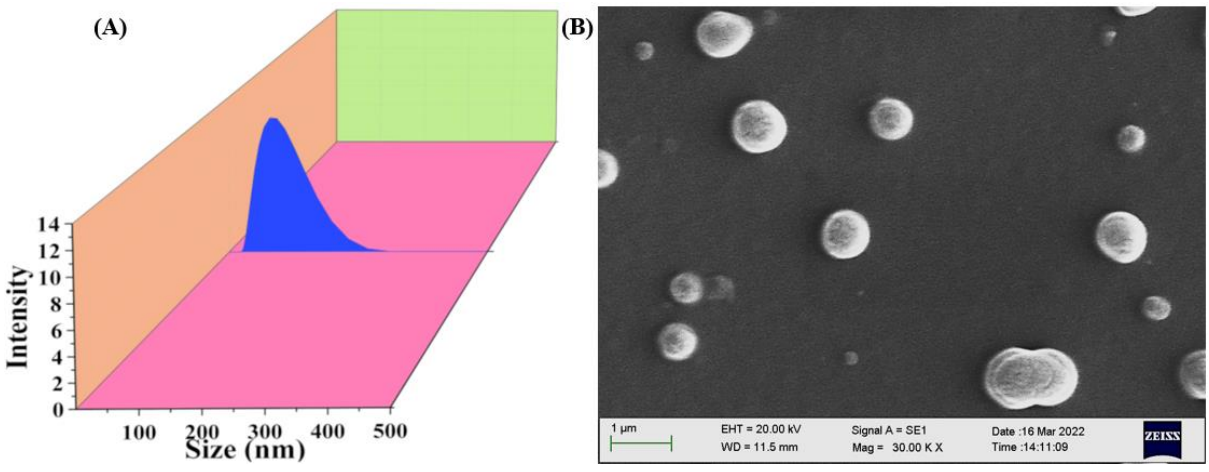

Figure 12: (A) Average particle size distribution of SLNs; (B) Scanning electron microscopy images of GEM-EGCG SLNs, which depict the surface properties of the formulation indicating spherical shape of GEM-EGCG SLNs

5.3.3 Percent entrapment efficiency

Percent entrapment efficiency for GEM-EGCG SLNs was determined by the equilibrium dialysis method and it was calculated as 95.035 ± 8.6 % for GEM and 92.406 ± 11.4 % for EGCG. High percent entrapment efficiency for GEM and EGCG could be accredited to the method of fabrication of GEM-EGCG SLNs which is the double emulsification solvent evaporation method. Both drugs are present in the inner hydrophilic core surrounded by a lipidic layer of GMS and HSPC followed by an outer hydrophilic layer of water in the W/O/W double emulsion [186]. According to 3-D contour plots (figure 10) for the percent entrapment efficiency of GEM and EGCG, the amount of phospholipid i.e., HSPC and surfactant has a considerable effect on the percent entrapment efficiency of both the drugs. HSPC has a direct correspondence with the percentage entrapment efficiency of GEM and EGCG which could be attributed to the interaction between them or accentuation of lipidic properties by HSPC in the oil phase of W/O/W double emulsion. It can be inferred that the surfactant must have provided better emulsification by decreasing the contact angle and surface tension to form a stable W/O/W double emulsion resulting in stable SLNs and better entrapment of drugs [187], [188].

5.3.4 Incompatibility study using Attenuated Total Reflectance (ATR)

ATR studies were conducted for GEM-EGCG SLNs, GEM, EGCG, GMS, Pluronic F-127, PVA, HSPC, and a physical mixture of GEM and EGCG. The ATR spectra (figure 13) for GEM-EGCG SLNs represent characteristic vibration peaks of -OH and NH_2 at 3366.37 cm^{-1} which corresponds to -OH bands of GMS and PVA at 3295.86 cm^{-1} and 3280 cm^{-}

[1]wavenumbers, respectively, and a stretching band for the -OH and amino groups of HSPC at wavenumber 3281.1 cm^{-1}. The other significant peaks attributed to symmetrical stretching of $-CH_3$ and $-CH_2$ are observed at wavenumbers 2914.57 cm^{-1} and 2849.27 cm^{-1} in the ATR spectra of GEM-EGCG SLNs which are also present in the ATR spectra of GMS, PVA, Pluronic F-127, and HSPC which symbolize that there is no interaction between these chemicals. The characteristic peaks of GEM at wavenumber 3059.51 cm^{-1}, 2976 cm^{-1}, 1671.09 cm^{-1}, and that of EGCG at wavenumbers 2361.11 cm^{-1}, 1540.74 cm^{-1}, and 1513.49 cm^{-1} and that of GMS at 1727 cm^{-1} representing C=O stretching are absent in the ATR spectra of GEM-EGCG SLNs which suggests the probability of conjugation or interaction between GEM, EGCG, and GMS [27], [74].

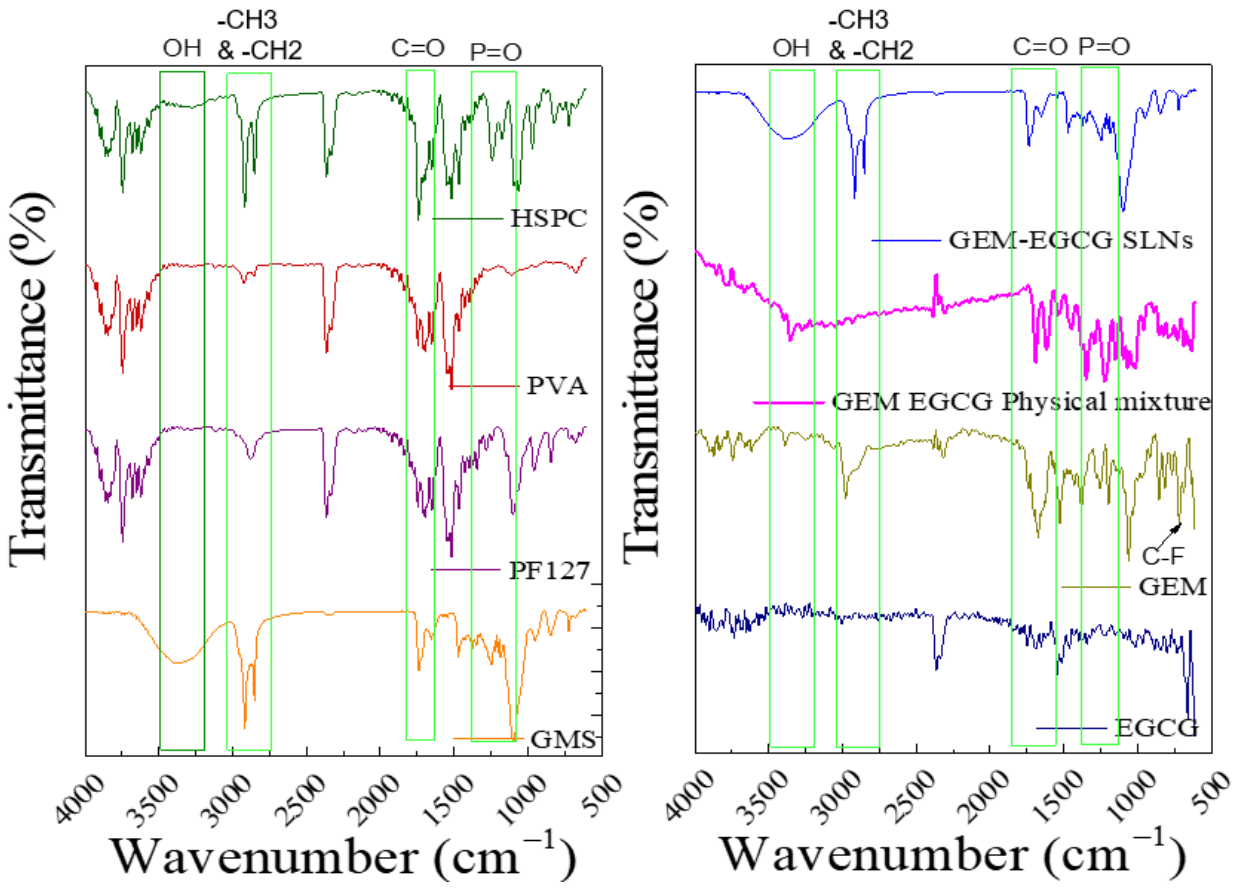

Figure 13: ATR graphs of pure GEM, pure EGCG, GMS, PF-127, PVA, HSPC, physical mixture of GEM and EGCG, and GEM-EGCG SLNs.

5.3.5 Thermogravimetric analysis

Thermogravimetric analysis is of great significance in determining thermal stability and percentage weight loss as a function of temperature. The weight loss curve of GEM (figure 14) depicts that it had a significant drop in weight after 280°C which is regarded as T_{max} (the temperature at which maximum decomposition or weight loss is observed) for pure GEM and decomposition rate was observed to be very low after 400°C. Further, we observed that EGCG had a significant weight loss from temperature 220-800°C whereas GMS depicted a degradation pattern from 20-400°C.The weight loss curve (figure 14) of GEM-EGCG SLNs formulation depicts a two-step degradation pattern that shows 5 % weight loss from 20°C to 250°C which could be attributed to the loss of adsorbed or bound water in the formulation [126], [189], [190]. The T_{max}, is observed at 250°C for GEM-EGCG SLNs and a noticeable weight loss of around 85 % was observed from 250°C to 420°C which could be due to the decomposition of organic groups of GEM and EGCG. It can be concluded from the data presented that the first threshold of weight loss was noticed from 20°C to 250°C. The other point in terms of stability of GEM-EGCG SLNs which could be inferred from the results of TGA analysis is that the formulation is deemed to be stable over a temperature range from room temperature to 250°C [191].

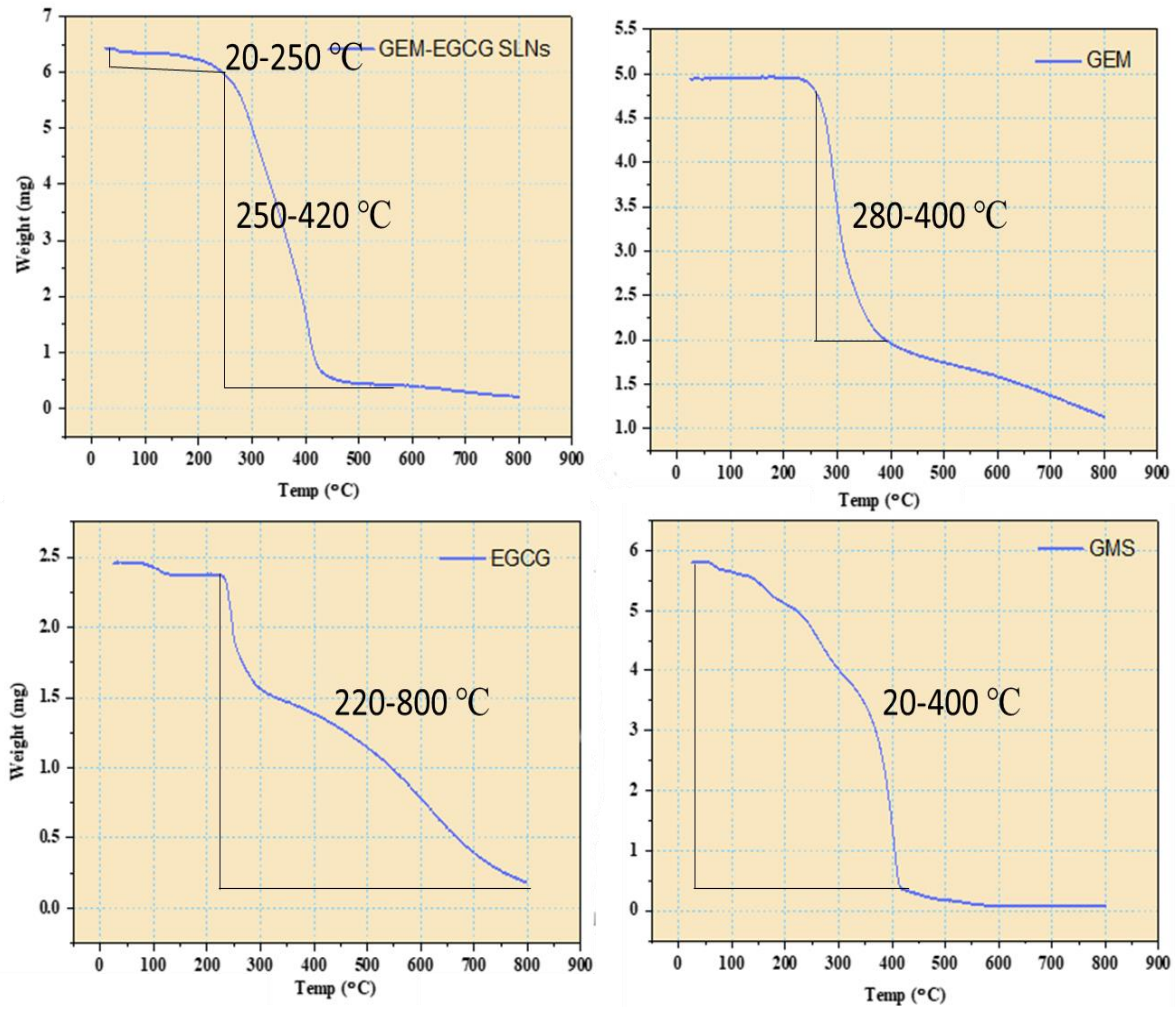

Figure 14: TGA graphs of GEM-EGCG SLNs, pure GEM, pure EGCG, and GMS, TGA graphs depict weight loss as a function of temperature.

5.3.6 Differential scanning calorimetry (DSC) analysis

DSC studies enable us to gain knowledge about interactions between excipients, GEM, and EGCG and its resultant effect on thermal properties. DSC curve is basically a graph between heat flow and temperature; (figure 15) indicating endothermic peak of GEM, at 300°C which corresponds to its melting point. The DSC curve for GEM represents crystallization (depicted by an exothermic peak) after the glass transition (or baseline shift) and subsequent

melting. DSC thermograms of pure EGCG typically display a small endothermic peak at 227 °C, which is indicative of its melting point. This peak reflects the transition of EGCG from a solid to a liquid state, providing valuable information about its thermal properties and purity [192]. When entrapped in SLNs the original peaks corresponded to the melting of GEM and EGCG and glass transition temperature were lost in the DSC curve for GEM-EGCG SLNs (figure 15). When GEM and EGCG are entrapped in SLNs, the original DSC peaks corresponding to the melting of both GEM and EGCG and the lipid matrix, as well as the glass transition temperature, are often lost or significantly altered. This indicates that the encapsulation process affects the thermal properties of the components, likely due to interactions between EGCG and the lipid matrix, leading to changes in their crystalline and amorphous states [193][194], [195], [196].

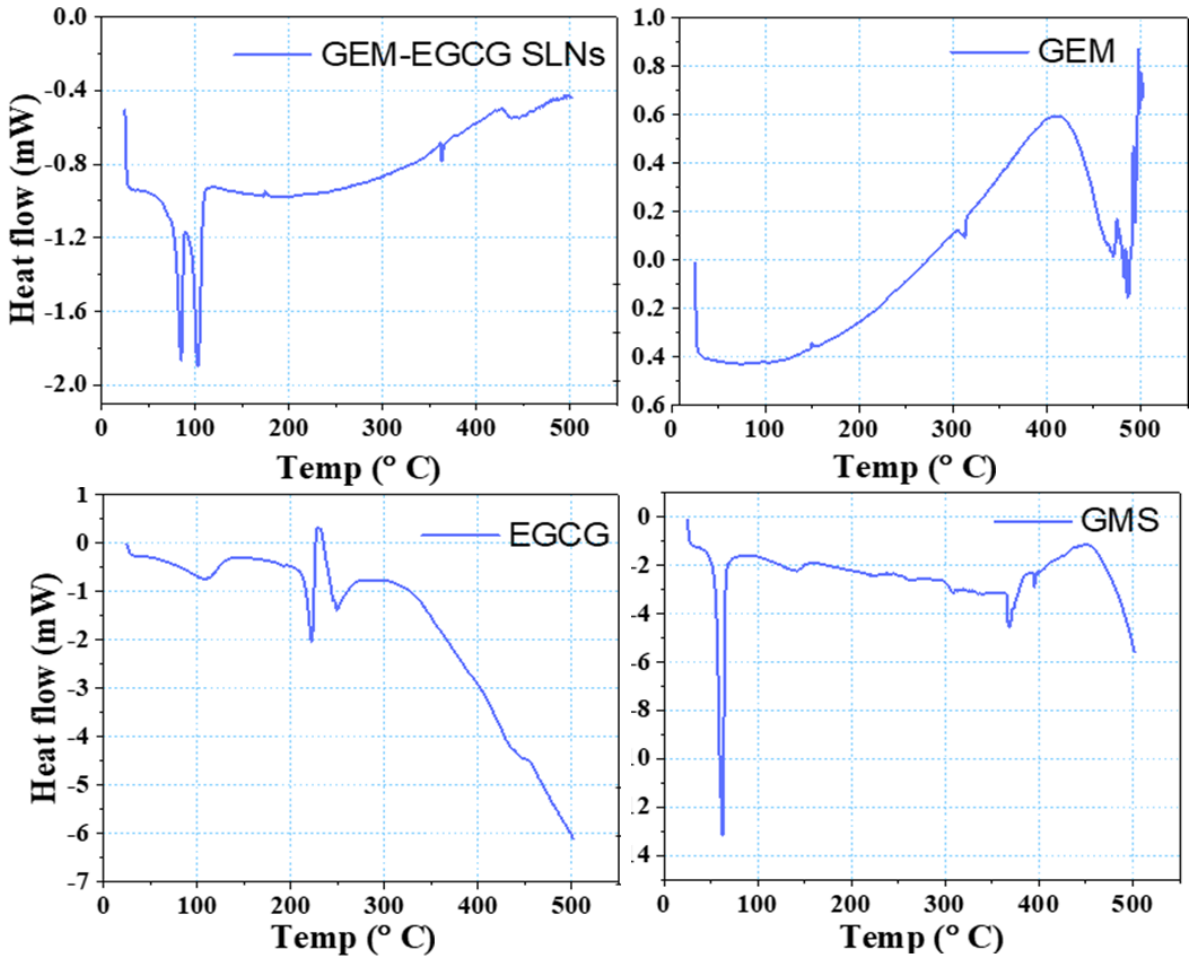

Figure 15: DSC graphs of GEM-EGCG SLNs, pure GEM, pure EGCG, and GMS.

5.3.7 In vitro release studies and kinetic models

It could be comprehended from the drug release data that the fabrication of gemcitabine and epigallocatechin-3-gallate loaded solid lipid nanoparticles showed a sustained release profile for GEM and EGCG. This could be attributed to the entrapment of GEM and EGCG in the inner hydrophilic core of the SLNs surrounded by a lipid layer. This whole arrangement of layers resulted in a sustained release of GEM and EGCG. From figure 16, it is coherent that a higher release of GEM occurred from GEM SLNs as compared to GEM-EGCG SLNs, this could be accounted for only one drug GEM being present in GEM SLNs whereas GEM-EGCG SLNs have two drugs (GEM as well as EGCG), which could alter the release of either of the drugs from SLNs into the release media. The same pattern has been noticed for EGCG SLNs and GEM-EGCG SLNs for the EGCG. Release kinetics was studied by fitting the release data in different drug release kinetic models viz., Zero order, First order, Higuchi, Hixson Crowell, and Korsemeyer Peppas. From the values of the correlation coefficient (R^2) (table 11 and figure 17 & 18), it can be suggested that the drug release profile of GEM-EGCG SLNs corresponds to the Higuchi model of drug release kinetics. This observation suggests that the drug release profile for GEM and EGCG from GEM-EGCG SLNs follows a release mechanism based on diffusion in accordance with the 'Fick's Law' [197].

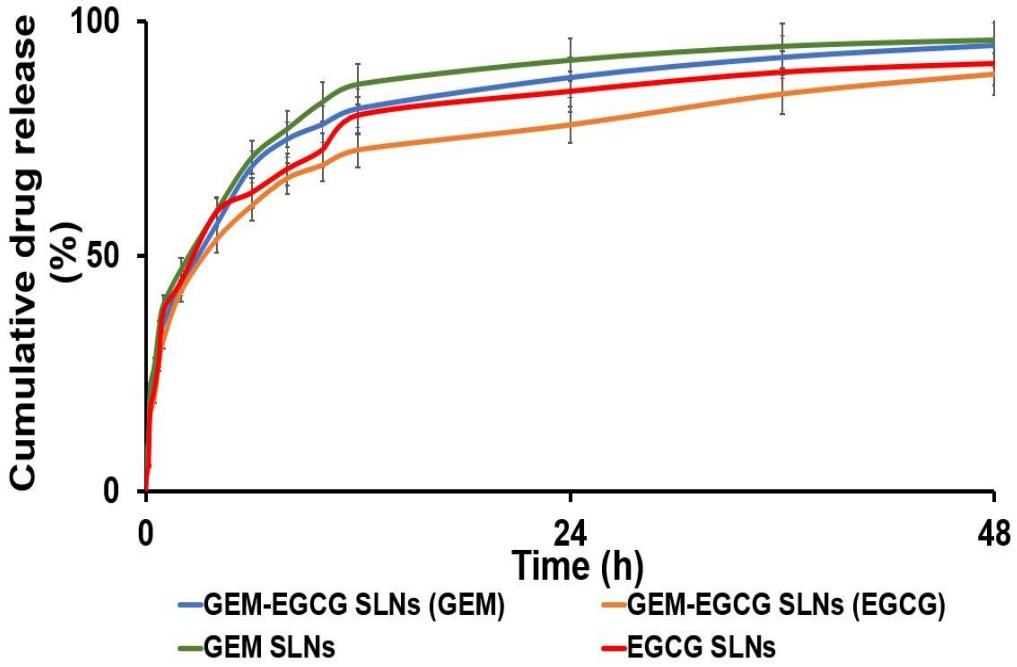

Figure 16: Cumulative percentage drug release profile of GEM-EGCG SLNs, GEM SLNs, and EGCG SLNs for the release of GEM and EGCG at pH 5.5 for a time period of 48 hours (the data has been presented as mean ± SD (n=3)).

Table 11: Correlation coefficient (R^2) values for different models at pH 5.5 for GEM and EGCG from GEM-EGCG SLNs.

S. No.	Release Kinetic Model	GEM	EGCG
1.	Zero order	0.6702	0.6829
2.	First order	0.8781	0.8431
3.	**Higuchi**	**0.9178**	**0.9244**
4.	Hixson Crowell	0.7818	0.7666
5.	Korsemeyer Peppas	0.9152	0.9066

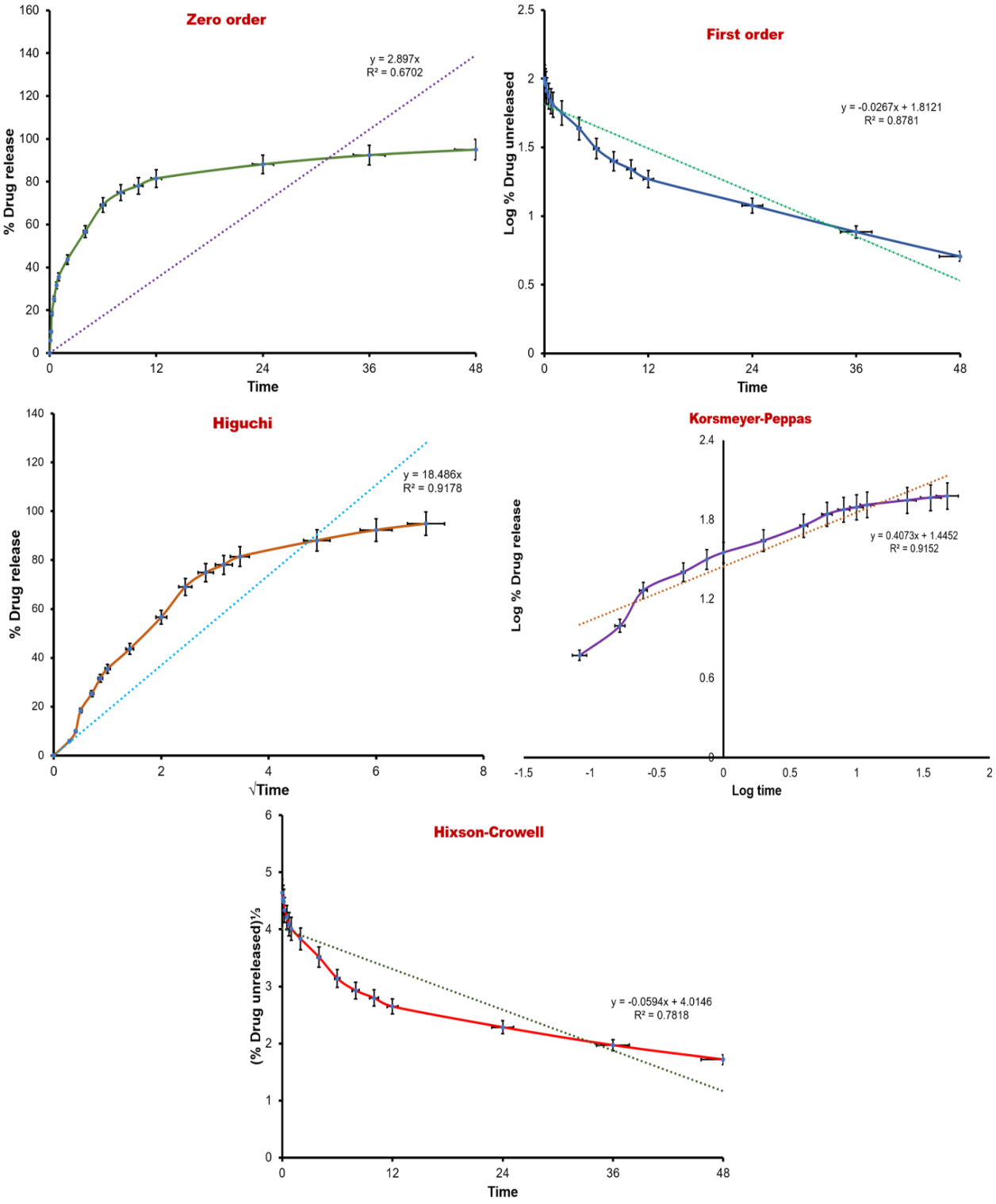

Figure 17: Release kinetics graphs of GEM from GEM-EGCG SLNs for release kinetic models viz., Zero order, First order, Higuchi, Hixson Crowell, and Korsemeyer Peppas at pH 5.5.

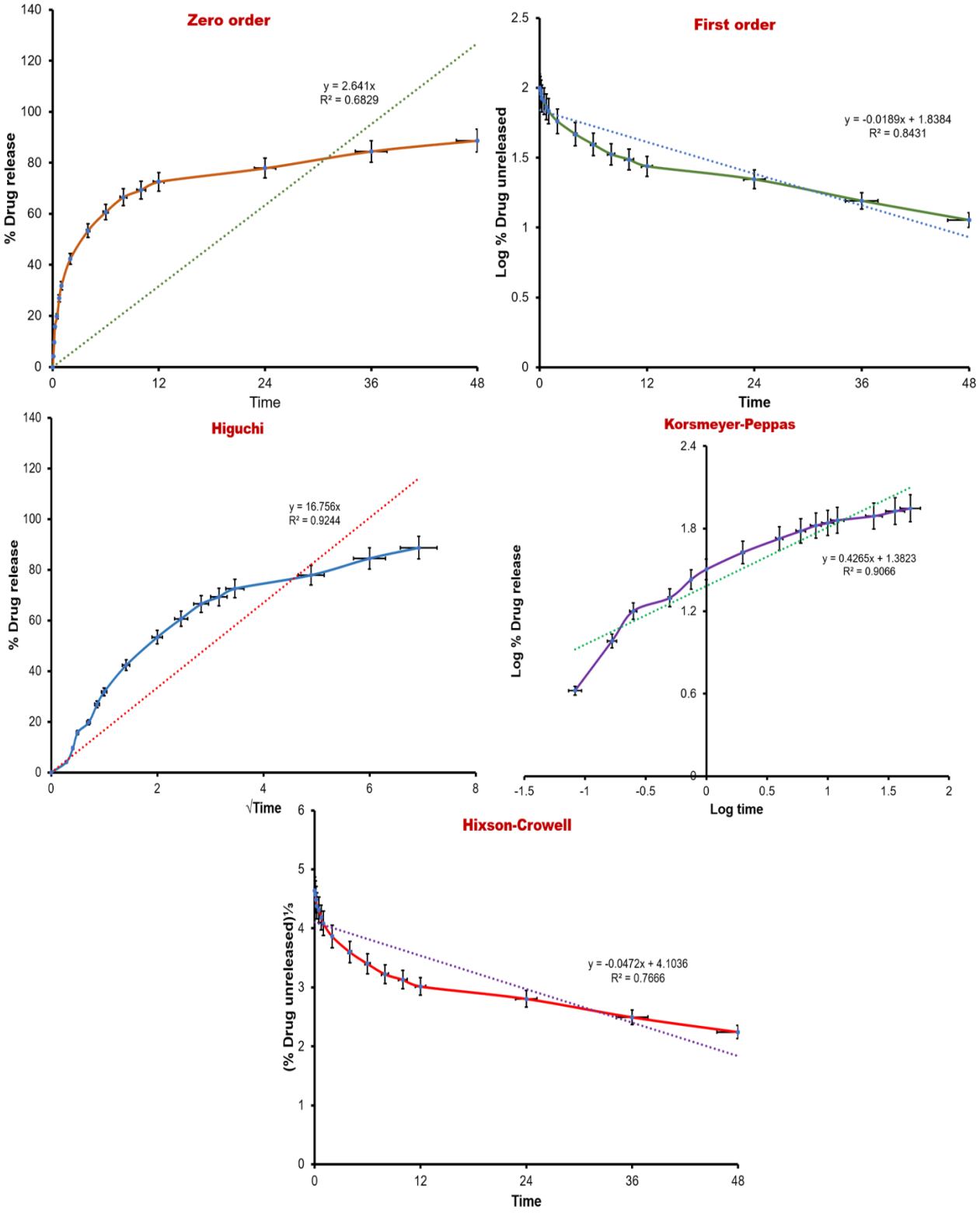

Figure 18: Release kinetics graphs of EGCG from GEM-EGCG SLNs for release kinetic models viz., Zero order, First order, Higuchi, Hixson Crowell, and Korsemeyer Peppas at pH 5.5.

5.4 *In vitro* cell line studies

5.4.1 Cytotoxicity assay

The principle of MTT assay is based on the mitochondrial activity of living cells which leads to the transformation of tetrazolium salt MTT into purple coloured formazan crystals, which is a direct indication of the mitochondrial activity and that is directly proportional to the number of viable cells [198]. It is comprehensible from figure 19, that a proportional decrease in the percent cell viability of A549 cells has been noticed with an increase in the concentration of GEM-EGCG SLNs, GEM SLNs, and EGCG SLNs. In contrast to this observed pattern, a non-significant change in the percent viability of A549 cells was observed for the GEM and EGCG as depicted by the purple and grey color in figure 19.

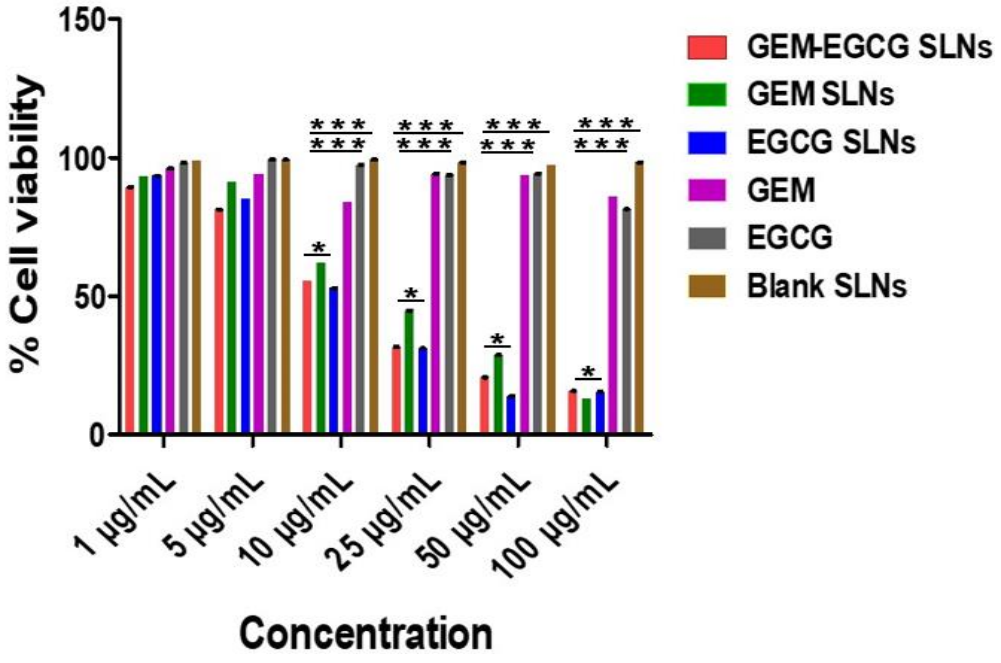

Figure 19: The % cell viability versus concentration graph for different formulations against A549 cell lines (the data has been presented as mean ± SD (n=3) and statistical values

represent ($*p < 0.05$), ($**p < 0.01$), ($***p < 0.001$) are statistically significant and ($p > 0.05$) non-significant (ns)).

The obvious reason that could be accounted for this observed pattern is the active internalization of nano-sized SLNs as compared to pure drugs, which resulted in a significant decrease in the percent cell viability [199]. Blanks SLNs exhibited almost null effect on the percent cell viability of A549 cells which led us to conclude that the constituents of SLNs have no cytotoxic effect on A549 cell lines. The IC_{50} value was found to be at 12.5 µg/mL, 18.5 µg/mL, and 11.4 µg/mL for GEM-EGCG SLNs, GEM SLNs, and EGCG SLNs as noticeable from figure 19, whereas GEM and EGCG were found to be inefficient at achieving the percent cell death to fifty percent [198].

Estimation of synergism (Combination index (CI))

The synergism in terms of the combination index between GEM and EGCG was calculated by the Chou Talalay method. A value of CI for 50% inhibition and 80% inhibition was found to be 0.91 and 0.392, respectively. The estimated values of CI (less than 1) depict a synergistic relationship between GEM and EGCG which is also comprehensive from the data of cytotoxicity assay. The value of the linear correlation coefficient (r) provides conformity to the data of the median effect principle (table 4).

5.4.2 Wound healing (scratch) assay

The metastatic potential of any tumor can be evaluated by its migration capability; hence, we have assessed the anti-migration efficacy of different formulations in A549 cell lines by wound healing assay [200]. From figure 20 (A), it can be seen that SLNs significantly averted the migration of A549 cells. It was observed that in the case of GEM-EGCG SLNs, about 85 % scratch wound area was uncovered after 48 hours of incubation at 5 µg/mL which was increased to around 90 % at 50 µg/mL. Whereas, in the case of GEM SLNs and EGCG SLNs

this value was 72 % and 74 %, respectively, at 50 µg/mL. The higher values of percent wound area was uncovered for GEM-EGCG SLNs as compared to GEM SLNs and EGCG SLNs warrant the combination potential of GEM and EGCG against inhibition of migration of A549 cells to prevent metastasis [139]. However, blank SLNs demonstrated only 2 % uncovering of wound area after 48 hours at both concentrations and the control group also depicted the same pattern as evident from figure 20 (B).

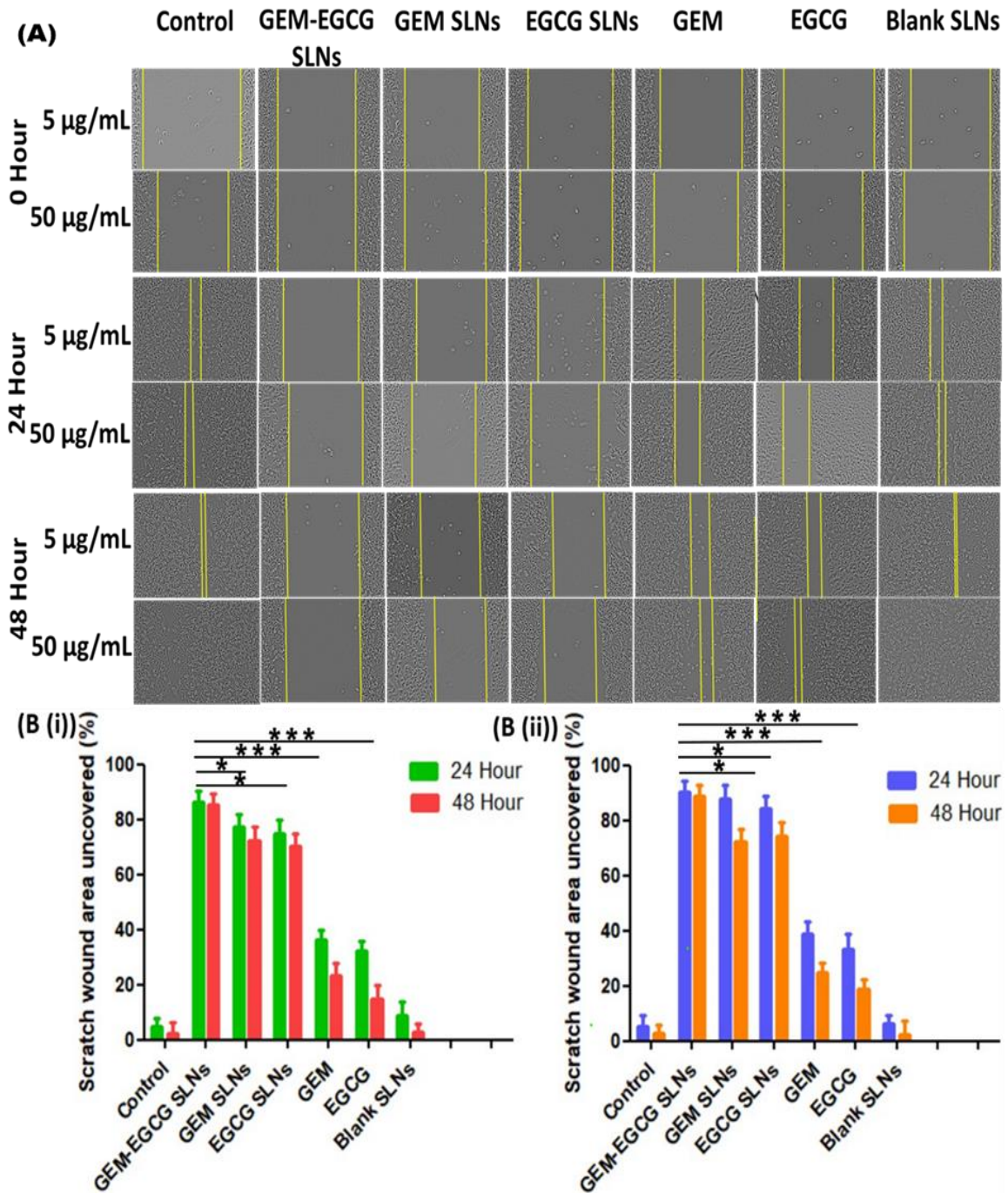

Figure 20: (A) Wound healing (scratch) assay depicting inhibitory potential of different treatments on A549 cell lines, (B) shows a bar graph of percent scratch wound area uncovered by cells after incubation for 24 hours and 48 hours at concentrations of 5 µg/mL (B(i)) and 50 µg/mL (B(ii)) of different treatments groups(the data has been presented as mean ± SD (n=3) and statistical values represent ($*p < 0.05$), ($**p < 0.01$), ($***p < 0.001$) are statistically significant and ($p > 0.05$) non-significant (ns)).

5.4.3 Cellular uptake studies

We conducted these studies to assess the potential of solid lipid nanoparticles (SLNs) for cellular uptake and their subsequent internalization into the nuclei of cells. The following observations were made:

Figure 21 illustrates that rhodamine, used as a marker, was not internalized into the nucleus of the cell. This is evident as black-colored nuclei are visible, and the presence of rhodamine is confined to the cytoplasm, as indicated by the red panel in row I and its merge with the blue DAPI panel.

However, SLNs demonstrated the capability to be internalized into the nuclei of cells. This conclusion is drawn from the merged images in rows II, III, IV, and V of figure 21, where the red panel (indicating SLNs) completely overlaps with the blue panel (indicating the nuclei stained with DAPI).

These results suggest that while rhodamine alone does not penetrate the cell nucleus, SLNs have the potential to be internalized and deliver their payload directly into the nucleus, which could be significant for drug delivery and therapeutic applications.

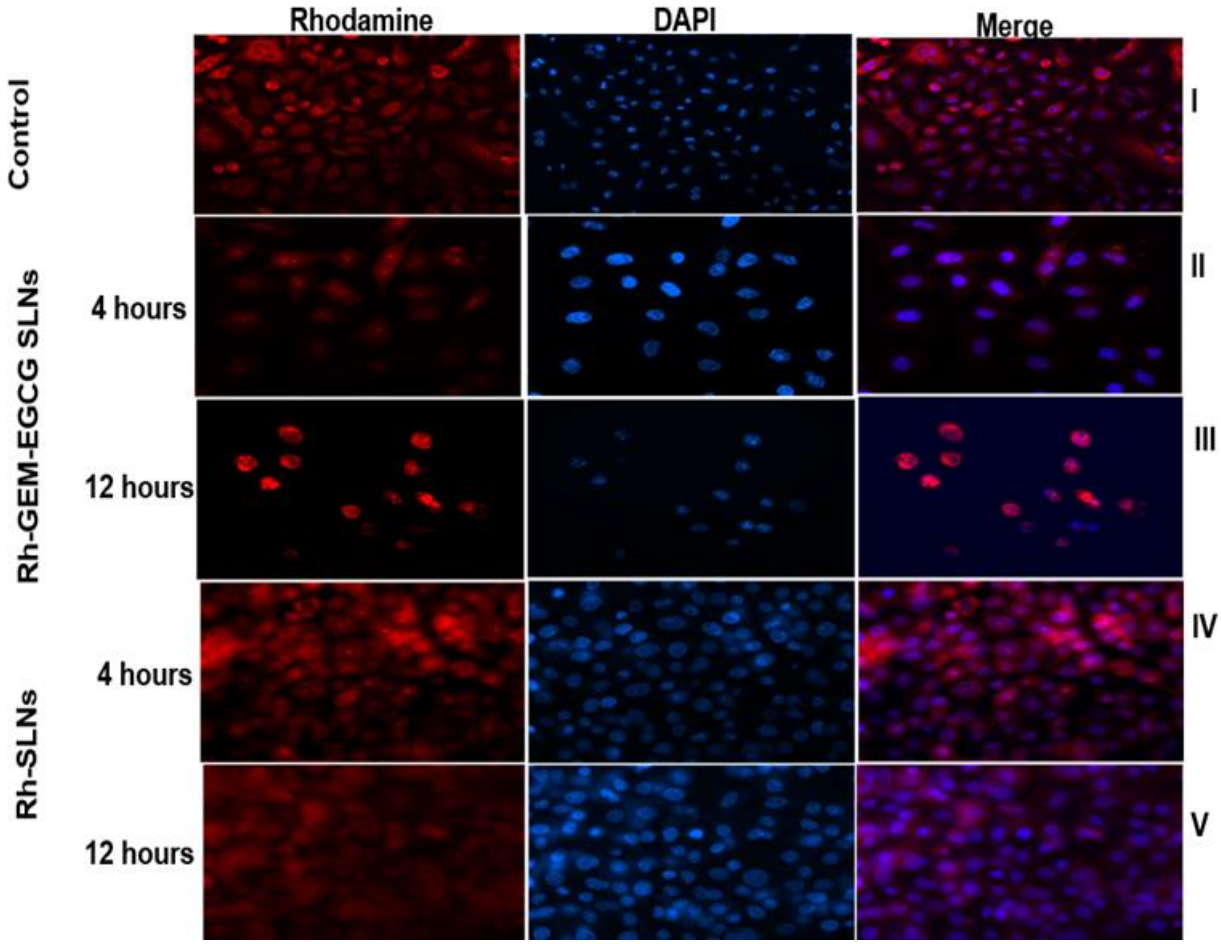

Figure 21: Fluorescence microscopy images of A549 cells depicting cellular uptake of rhodamine-tagged GEM-EGCG SLNs (Rh-GEM-EGCG SLNs) and rhodamine-tagged SLNs (Rh-SLNs) at 4 and 12 hours.

The internalization of solid lipid nanoparticles (SLNs) into nuclei can be attributed to their small size in the nanometer range. This size allows for efficient uptake and transport within cells. Observations at different time points revealed that at 12 hours, there was a greater intensity of the red panel in the nuclei for Rh-GEM-EGCG SLNs (as seen in row III of figure 21) compared to 4 hours (row II of figure 21). At 4 hours, Rh-GEM-EGCG SLNs were visible both in the cytoplasm and nuclei, indicating that they were initially distributed throughout the cell. Over time, the nanoparticles gradually accumulated more within the nuclei, suggesting a time-dependent uptake process. This gradual internalization is crucial as

it leads to a sustained cytotoxic effect against A549 cells. By localizing within the nucleus, the Rh-GEM-EGCG SLNs can exert their therapeutic effects more effectively, enhancing the overall efficacy of the treatment [30], [201].

5.4.4Annexin V FITC/PI apoptosis assay

Annexin V FITC/PI assay for determination of the rate of apoptosis was performed to explore the mechanism of antiproliferative potential of GEM-EGCG SLNs against A549 cell lines [144]. From figure 22, it is evident that GEM-EGCG SLNs had a higher degree of growth inhibition in A549 cell lines via induction of apoptosis as compared to mono treatment groups viz., GEM SLNs and EGCG SLNs. GEM-EGCG SLNs exhibited an apoptotic rate of 29.72 % in the late apoptotic phase whereas 34.33 % in the early apoptotic phase with 7.83 % of the necrotic phase. The results demonstrate the synergistic effect of EGCG and GEM on the induction of apoptosis in A549 cells. For all other formulations viz., GEM SLNs, EGCG SLNs, GEM, and EGCG apoptotic rate was less as compared to GEM-EGCG SLNs (figure 22). GEM and EGCG have shown an apoptotic rate of less than 10 % which could be due to less internalization or cellular uptake in the A549 cells as compared to GEM-EGCG SLNs, GEM SLNs, and EGCG SLNs which have particle sizes in the nanometer range and hence are efficiently internalized in the A549 cells which of course resulted in their higher apoptotic activity [30]. The high apoptotic rate shown by GEM-EGCG SLNs depicts efficient anti-tumor activity against A549 cells as compared to other treatment groups [29]. To further assess the mechanism of apoptosis, ROS production was quantified by flow cytometer (CytoFLEX, Beckman coulter, Life sciences).

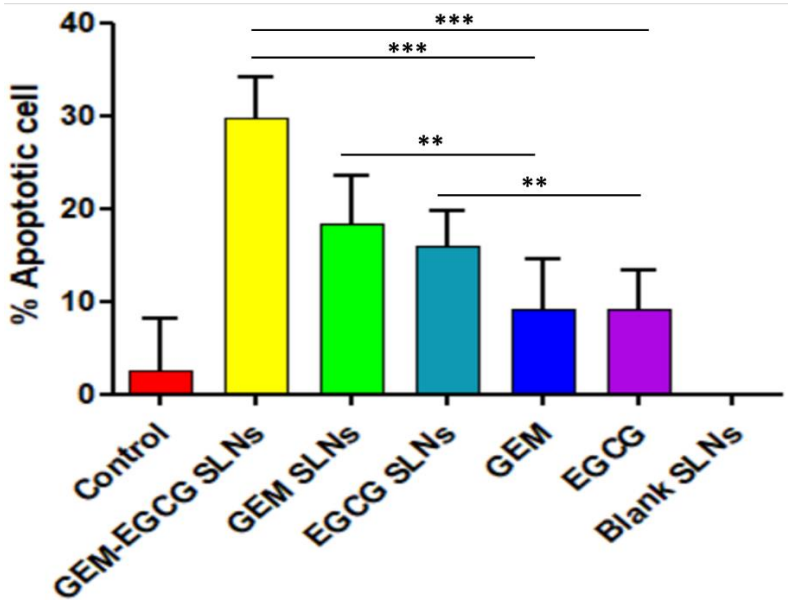

Figure 22: Bar graph depicting the percent apoptotic cell death by different formulations(the data has been presented as mean ± SD (n=3) and statistical values represent ($*p < 0.05$), ($**p < 0.01$), ($***p < 0.001$) are statistically significant and ($p > 0.05$) non-significant (ns)).

5.4.5 Reactive oxygen species (ROS) assay

One of the main mechanisms that contributes to tumor resistance is the low level of ROS in cancer stem cells which is important for the maintenance of these stem cells. Cancer stem cells act as a reservoir of cancerous cells and lead to recurrence of cancer even after treatment. Hence, high levels of ROS could negatively affect the survival of cancer stem cells which will thereby prevent reversal of cancer treatment [202]. Also, cancer cells undergo various stresses that lead to oxidative injury and the production of ROS also induce apoptosis of cancer cells [145]. Hence, we quantified ROS levels in A549 cells after treatment with GEM-EGCG SLNs, GEM SLNs, EGCG SLNs, GEM, EGCG, and blank SLNs with a flow cytometer using the DCFDA fluorescence dye method. We found the highest levels of ROS production in the case of GEM-EGCG SLNs (figure 23) which are in accordance with the results of cytotoxicity assay whereas GEM SLNs and EGCG SLNs exhibited comparable

levels of ROS production. Based on this study it can be suggested that ROS production mediated the anti-proliferative action of GEM-EGCG SLNs in A549 cells [203].

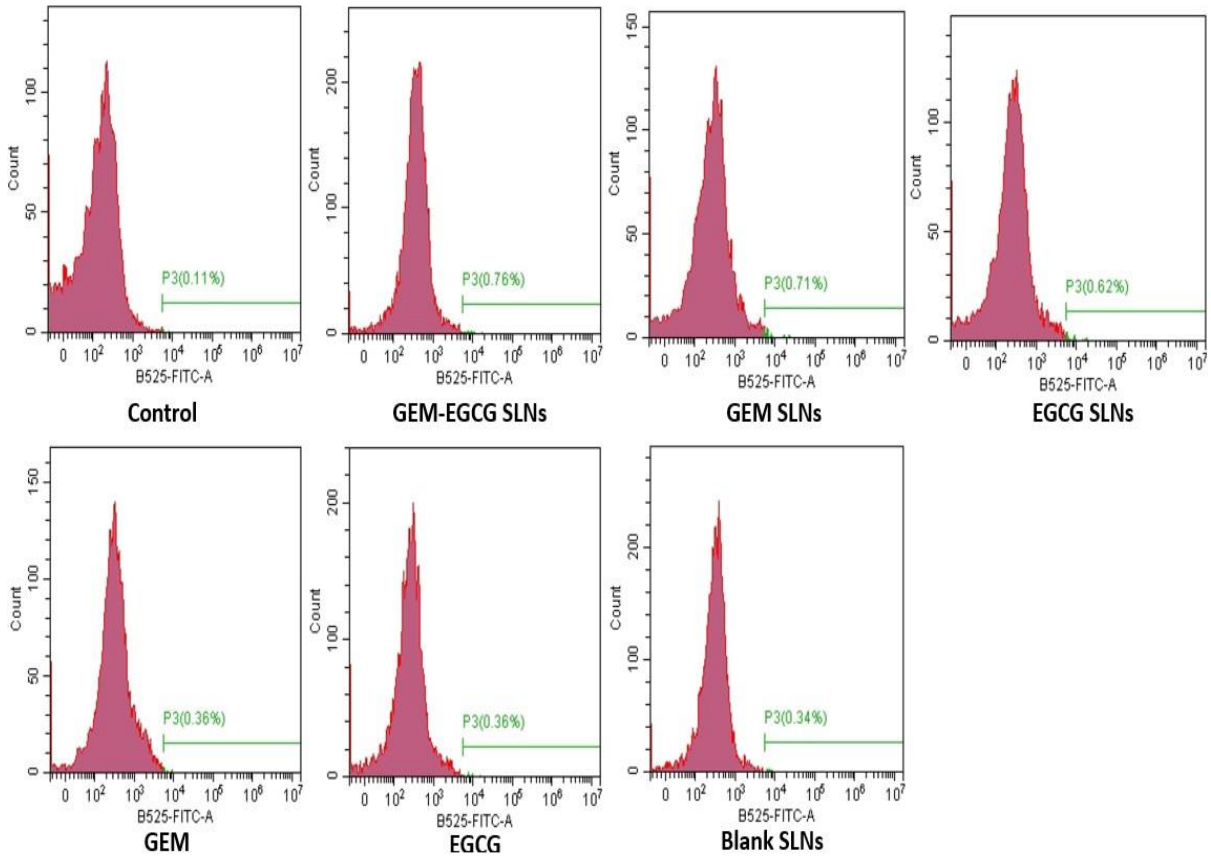

Figure 23: ROS graphs of different formulations depicting percentage of ROS generation.

The experimental data obtained from *in vitro studies* collectively suggest that GEM and EGCG synergize through enhanced cellular uptake via SLNs, leading to improved anti-tumorigenic and anti-proliferative effects. This synergy manifests as:

More efficient tumor cell killing, reflected by a significant drop in viability and lower IC50 values. The lower IC50 value of GEM-EGCG SLNs (11.4 µg/mL) compared to GEM SLNs (18.5 µg/mL) and EGCG SLNs (12.5 µg/mL) demonstrates enhanced potency of the combination, indicating a synergistic suppression of tumor cell growth beyond additive effects. Stronger inhibition of cancer cell migration, indicative of anti-metastatic and anti-

angiogenic potential. Elevated ROS disrupts cellular redox balance, causing oxidative stress that triggers apoptosis and inhibits cancer stem cell survival, potentially preventing tumor recurrence. Given that ROS and oxidative stress can inhibit angiogenesis by damaging endothelial cells and reducing pro-angiogenic factors, the increased ROS production by GEM-EGCG SLNs likely contribute indirectly to anti-angiogenic effects. The enhanced inhibition of A549 cell migration further suggests disruption of processes essential for angiogenesis and metastasis, reinforcing the anti-angiogenic potential of the combination. Higher induction of apoptosis and ROS-mediated oxidative stress, further undermine tumour cell survival and stem cell maintenance.

Thus, the combination therapy delivered by SLNs represent a promising strategy to tackle lung cancer via multiple anticancer pathways, achieving superior efficacy over individual agents.

5.5 Stability studies

The stability studies for GEM-EGCG SLNs were carried out for a period of 3 months and particle size, PDI, zeta potential, and percent entrapment efficiency were measured at 0, 1, 2, and 3 months duration as listed in table 12. We found that GEM-EGCG SLNs were stable for the observation period of 3 months with only slight changes in the values of particle size, PDI, zeta potential, and percent entrapment efficiency, however, long-term stability studies are required for better understanding. The change in percent entrapment efficiency over the period of 3 months was found to be very less which is the characteristic of solid lipid nanoparticles as solid lipid matrix provides efficient entrapment of drug, especially hydrophilic drugs like GEM or EGCG find it difficult to leach out, supplemented by the presence of phospholipids in GEM-EGCG SLNs. This could be the possible reason for the appreciable stability of GEM-EGCG SLNs [204], [205].

Table 12: Stability data of GEM-EGCG SLNs for 3 months for the characteristic particle size, PDI, zeta potential, and percent entrapment efficiency (the data has been presented as mean ± SD (n=3))

Months	Particle size	PDI	Zeta Potential	% Entrapment efficiency
0	122.8 ± 8.02 nm	0.1738 ± 0.02	-35.9 ± 1.6 mV	95.035 ± 8.6 % for GEM and 92.406 ± 11.4 % for EGCG
1	128.6 ± 8.58 nm	0.191 ± 0.05	-32.7 ± 2.1 mV	93.965 ± 10.6 % for GEM and 91.246 ± 8.8 % for EGCG
2	134.1 ± 9.17 nm	0.218 ± 0.02	-29.3 ± 1.8 mV	92.035 ± 7.4 % for GEM and 90.676 ± 9.2 % for EGCG
3	141.4 ± 7.21 nm	0.251 ± 0.03	-24.6 ± 1.3 mV	90.345 ± 9.1 % for GEM and 89.706 ± 12.4 % for EGCG

5.6 Pharmacokinetic study

5.6.1 Pharmacokinetics (Lung & Plasma)

Female Wistar rats, 250 g ± 10 g, were employed to study the pharmacokinetic profiles of GEM-EGCG SLNs, GEM SLNs, EGCG SLNs, pure GEM solubilized in PBS 7.4, and pure EGCG solubilized in PBS 7.4 in plasma and lungs. The various pharmacokinetic parameters for GEM and EGCG in plasma and lungs were evaluated by Kinetica 5.0 PK/PD Analysis software (Thermo Fisher Scientific). The various pharmacokinetic parameters have been

mentioned in Table 13 and Table 14. It was found that GEM-EGCG SLNs showed an 18.2-fold increase in $t_{1/2}$ as compared to pure GEM and a 9.2-fold increase concerning GEM SLNs for the drug GEM. Whereas for the drug EGCG, GEM-EGCG SLNs showed an increase of 1.62-fold and 8.9-fold in the $t_{1/2}$ concerning EGCG SLNs and pure EGCG, respectively. The increase in the $t_{1/2}$ (which is defined as the time required for half of the drug to be excreted out from the body) could be accounted for by the sustained release of GEM and EGCG into the plasma from the SLNs.

Table 13: Pharmacokinetic parameters for GEM and EGCG in plasma upon intranasal administration (the data has been presented as mean ± SD (n=3)).

S.No.	**Drug**	**Formulation**	**T_{max} (h)**	**C_{max}(µg /mL)**	**$t_{½}$ (h)**	**MRT (h)**	**Clearance (mL/h)**	**V_D (L)**	**AUC (µg/µL*h)**
1.	GEM (Plasma)	GEM-EGCG SLNs	1	37.44	272.4	386.92	0.298	0.12	2.514
		GEM SLNs	1	43.05	29.7	22.85	3.101	0.27	0.249
		Pure GEM	0.5	79.63	14.9	19.49	7.642	0.33	0.098
2.	EGCG (Plasma)	GEM-EGCG SLNs	0.5	36.50	94.9	134.06	1.872	0.198	2.003
		EGCG SLNs	0.5	44.39	58.7	81.68	2.339	0.247	1.603
		Pure EGCG	0.5	84.29	10.7	10.34	16.020	0.256	0.234

(Abbreviations: GEM- gemcitabine; EGCG- epigallocatechin-3-gallate; GEM-EGCG SLNs- gemcitabine and epigallocatechin-3-gallate loaded solid lipid nanoparticles; GEM SLNs- gemcitabine loaded solid lipid nanoparticles; EGCG SLNs- epigallocatechin-3-gallate loaded solid lipid nanoparticles)

Table 14: Pharmacokinetic parameters for GEM and EGCG in lungs upon intranasal administration (the data has been presented as mean ± SD (n=3)).

S.No.	**Drug**	**Formulation**	**T_{max} (h)**	**C_{max} (µg/mL)**	**$t_{½}$ (h)**	**MRT (h)**	**Clearance (mL/h)**	**AUC (µg/µL*h)**
1.	GEM (Lungs)	GEM-EGCG SLNs	0.5	35.01	87.7	126.40	0.261	2.871
		GEM SLNs	0.5	38.24	18.4	27.03	0.926	0.810
		Pure GEM	0.083	61.20	1.2	1.48	1.174	0.064
2.	EGCG (Lungs)	GEM-EGCG SLNs	0.5	43.27	8.0	11.76	7.421	0.505
		EGCG SLNs	0.5	50.95	7.7	11.31	6.638	0.565
		Pure EGCG	0.083	72.44	2.0	2.81	18.781	0.201

(Abbreviations: GEM- gemcitabine; EGCG- epigallocatechin-3-gallate; GEM-EGCG SLNs- gemcitabine and epigallocatechin-3-gallate loaded solid lipid nanoparticles; GEM SLNs- gemcitabine loaded solid lipid nanoparticles; EGCG SLNs- epigallocatechin-3-gallate loaded solid lipid nanoparticles)

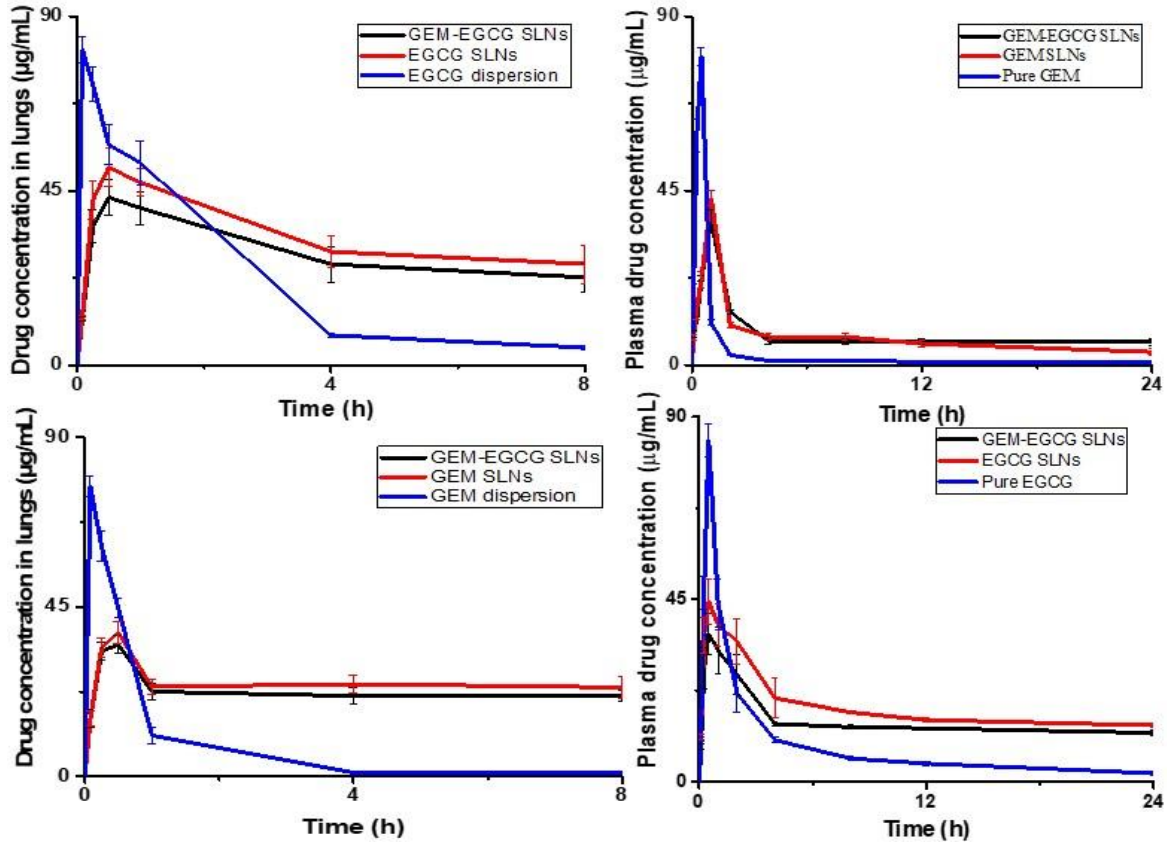

Figure 24: Pharmacokinetic profile of GEM and EGCG in plasma and lungs for GEM-EGCG SLNs, GEM SLNs, EGCG SLNs, pure GEM, and pure EGCG, the data has been presented as mean ± SD (n=3).

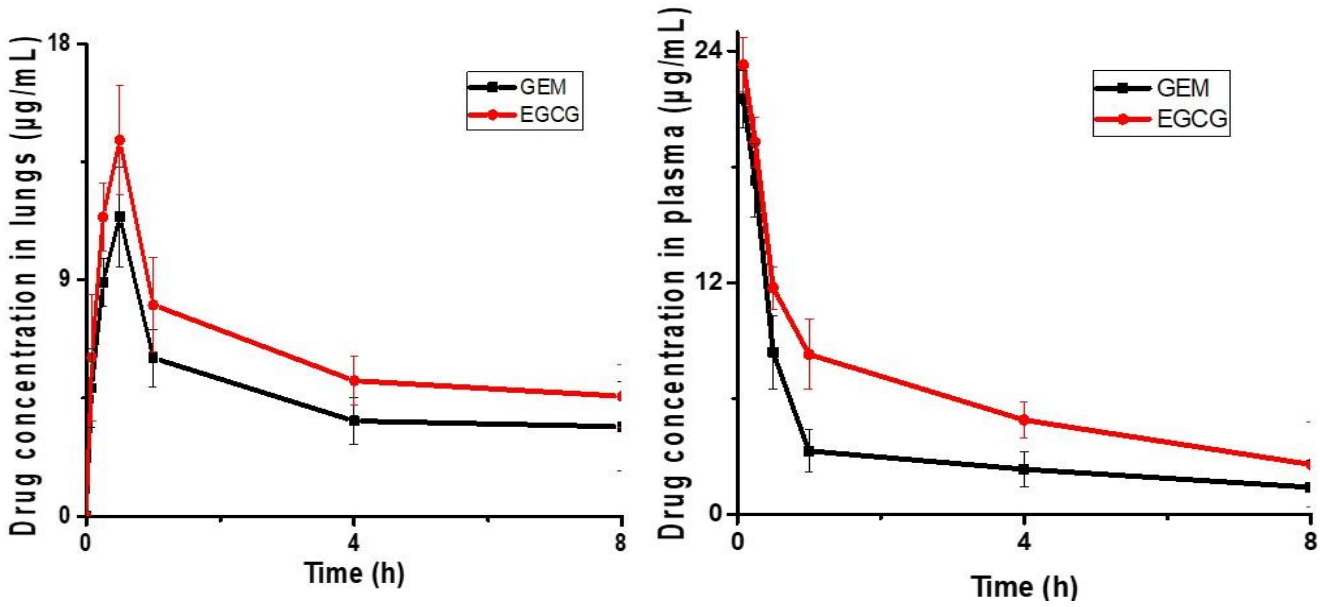

Figure 25: Pharmacokinetic profile of GEM and EGCG in lungs and plasma of mice after intravenous bolus administration of GEM-EGCG SLNs, the data has been presented as mean ± SD (n=3).

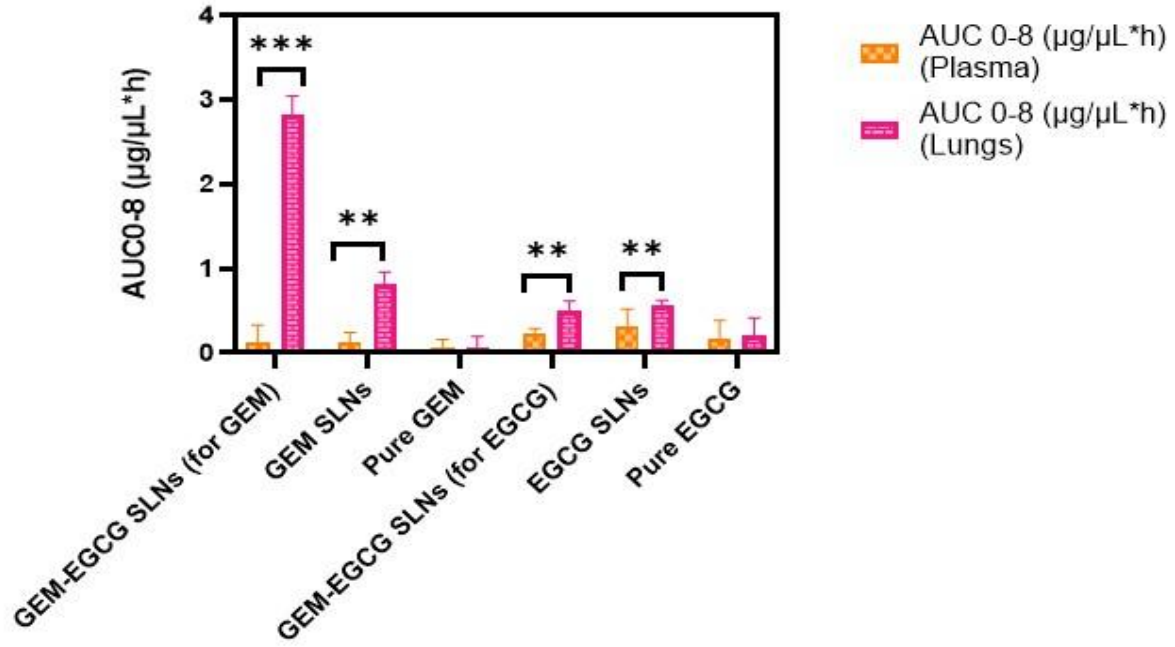

Figure 26: Graphical representation of the comparison of $AUC_{0\text{-}8}$ for different formulations in plasma and lungs upon intranasal administration (the data has been presented as mean ± SD (n=3) and statistical values represent ($*p < 0.05$), ($**p < 0.01$), ($***p < 0.001$) are statistically

significant and ($p > 0.05$) non-significant (ns)) (abbreviations: GEM- gemcitabine; EGCG- epigallocatechin-3-gallate; GEM-EGCG SLNs- gemcitabine and epigallocatechin-3-gallate loaded solid lipid nanoparticles; GEM SLNs- gemcitabine loaded solid lipid nanoparticles; EGCG SLNs- epigallocatechin-3-gallate loaded solid lipid nanoparticles)

Similarly, mean residence time (MRT) showed a pattern similar to that of $t_{1/2}$ for different formulations. It is comprehensible from Table 1 that for the drug GEM, an approximately 17 times increase in MRT was noticed for GEM-EGCG SLNs as compared to GEM SLNs, and 19.85-fold higher MRT for GEM-EGCG SLNs for pure GEM was observed. For EGCG a 1.64-fold escalation in MRT was observed for GEM-EGCG SLNs in comparison to EGCG SLNs and 12.9-fold for GEM-EGCG SLNs and pure EGCG. An escalation in the values of MRT for GEM-EGCG SLNs could be attributed to the long circulation of these nanoparticles in the systemic circulation due to the enhanced permeability and retention (EPR) effect and sustained and regulated release of these drugs from the SLNs into the bloodstream [28]. A better pharmacokinetic profile can improve the therapeutic activity of the drugs. The slower the rate of clearance of a drug from the body, the better the chances for a good therapeutic effect because the drug will be available for a longer duration of time in the body. In other words, MRT and rate of clearance have an inverse relation between them. GEM-EGCG SLNs showed a 10-fold decrease in the rate of clearance in comparison to GEM SLNs whereas, from table 13, it is evident that for the drug EGCG, a fall off of 1.25 and 8.56-fold respectively was observed for GEM-EGCCG SLNs in comparison to EGCG SLNs and pure EGCG. A 2.25 and 2.75-fold decline in the volume of distribution (V_D) was observed for GEM-EGCG SLNs in comparison to GEM SLNs and pure GEM, respectively for the drug GEM, whereas, for the drug EGCG, GEM-EGCG SLNs showed 1.21 and 1.29-fold decrease for EGCG SLNs and pure EGCG. The fall in the value of V_D for GEM-EGCG SLNs indicates lower biodistribution and in turn would probably lead to lower associated toxicity of GEM

and EGCG in various body organs which in turn also indirectly corroborates the targeting efficiency of intranasal administration of GEM-EGCG SLNs into lungs. The value of area under the curve (AUC) was found to be the highest for GEM-EGCG SLNs in the case of both the drugs i.e., GEM and EGCG concerning GEM SLNs, EGCG SLNs, pure GEM, and pure EGCG. Higher AUC supports the slower clearance of drugs from the body and greater residence of the drugs in the body.

Table 14 enlists different Pharmacokinetic parameters for GEM and EGCG in the lungs upon intranasal administration, it is comprehensible that C_{max} in the lungs was attained faster as compared to that of plasma suggesting faster onset of action of GEM and EGCG in the lungs. From figure 26, it can be seen that an escalation in the value of AUC_{0-8} (AUC for the time points 0-8 hours) was noticed for GEM and EGCG in the lungs as compared to that of plasma for the drug-loaded SLNs formulations (GEM-EGCG SLNs, GEM SLNs, and EGCG SLNs). This could be due to a slower rate of clearance from the lungs or re-entry of GEM and EGCG into the lungs via the pulmonary artery from the heart [206].

5.7 Lung targeting efficiency of intranasal route

5.7.1 Drug Targeting Index

DTI was quantified for GEM-EGCG SLNs in lungs and plasma upon intranasal and intravenous administration (figure 25). The quantification of DTI for GEM-EGCG SLNs in both lungs and plasma upon intranasal and intravenous administration provides crucial insights into their effectiveness. The DTI values indicate a significant advantage of intranasal administration over the intravenous route, with GEM showing a DTI of 17.605 and EGCG a DTI of 2.118. According to existing reports, a DTI greater than 1 signifies that the drug predominantly reaches the target site.[52]. The DTI values suggest that intranasal delivery of GEM-EGCG SLNs is more efficient in targeting lung tissue compared to intravenous

administration. This is likely because intranasal administration bypasses the first-pass metabolism that occurs in the liver, allowing more of the drug to reach the target site. This approach is non-invasive and patient compliant. GEM exhibited a substantially higher DTI when administered intranasally. This can be attributed to the fact that intravenously administered GEM is rapidly distributed to various body organs and degraded by plasma deaminase. Additionally, it is eliminated by the liver and kidneys. In contrast, intranasal administration allows for a greater concentration of GEM to accumulate in the lungs. In comparison to GEM, the DTI value for EGCG is quite less which could account for the less biodistribution and elimination of EGCG after intravenous administration as compared to GEM [52], [160]. The findings indicate that intranasal administration of GEM-EGCG SLNs could serve as a targeted therapeutic approach for treating lung cancer. This method offers a non-invasive alternative that enhances patient compliance and ensures higher drug concentrations at the target site, thus potentially improving therapeutic outcomes. By maximizing drug concentration at the target site and minimizing systemic exposure, this method holds promise for improving treatment outcomes and reducing side effects.

5.7.2 IVIS- In vivo imaging system

To evaluate the efficiency of the intranasal route for targeting the lungs, IVIS was used. IVIS is a powerful tool used to study the biodistribution and pharmacokinetics of drug delivery systems in live animals. This technique allows for real-time, non-invasive tracking of nanoparticles within the body.

The following findings were made from figure 27 (A):

1. **0 Hours: Initial Accumulation in Lungs**: At the initial time point (0 hours), GEM-EGCG SLNs were predominantly located in the lungs. This immediate localization suggests that the intranasally administered nanoparticles are efficiently transported to

and retained within the lung tissue. The nasal cavity provides a direct route to the lungs, bypassing systemic circulation and delivering a high concentration of the drug to the target site.

2. **1 Hour: Presence in Liver Region**: By 1 hour post-administration, the nanoparticles began to appear in the liver region. The liver is a primary organ for drug metabolism and clearance. The appearance of GEM-EGCG SLNs in the liver indicates that some of the nanoparticles are being processed by the body's detoxification system. This is a common phenomenon, as the liver tends to filter and process substances entering the bloodstream.

3. **2 Hours Onwards: Uptake by RES (Kidney, Intestines, and Spleen):** Starting from the 2nd hour, GEM-EGCG SLNs were found in the kidney, intestines, and spleen. The reticuloendothelial system (RES) is responsible for phagocytosing and clearing foreign particles. The distribution of nanoparticles to the RES organs (kidney, intestines, spleen) indicates their uptake and processing by immune cells, which is a natural response to foreign substances in the bloodstream.

4. **24 and 48 Hours: Sustained Presence in Lungs**: Even at 24 and 48 hours post-administration, GEM-EGCG SLNs were detected in the lungs. The sustained presence of nanoparticles in the lungs suggests a prolonged release profile. This is significant for therapeutic applications, as it means that the drug can exert its effects over an extended period, reducing the need for frequent dosing and enhancing patient compliance. The slow release of GEM-EGCG SLNs ensures that therapeutic levels of the drug are maintained in the target tissue for a longer duration.

The results confirm that intranasal administration is an effective route for targeting the lungs. This method ensures high drug concentration at the target site, maximizing therapeutic

efficacy while minimizing systemic side effects. The prolonged presence of nanoparticles in the lungs is indicative of a sustained release mechanism. This is beneficial for treatments requiring long-term drug exposure at the site of action, such as in the case of lung cancer. Intranasal administration is non-invasive and easier for patients to use, which can improve adherence to treatment protocols.

The IVIS imaging data provides strong evidence supporting the use of intranasal administration for delivering GEM-EGCG SLNs to the lungs. This route not only ensures efficient targeting and prolonged drug release but also offers a patient-friendly alternative to invasive administration methods. The observed distribution pattern highlights the potential of this approach in enhancing the effectiveness of lung cancer therapies.

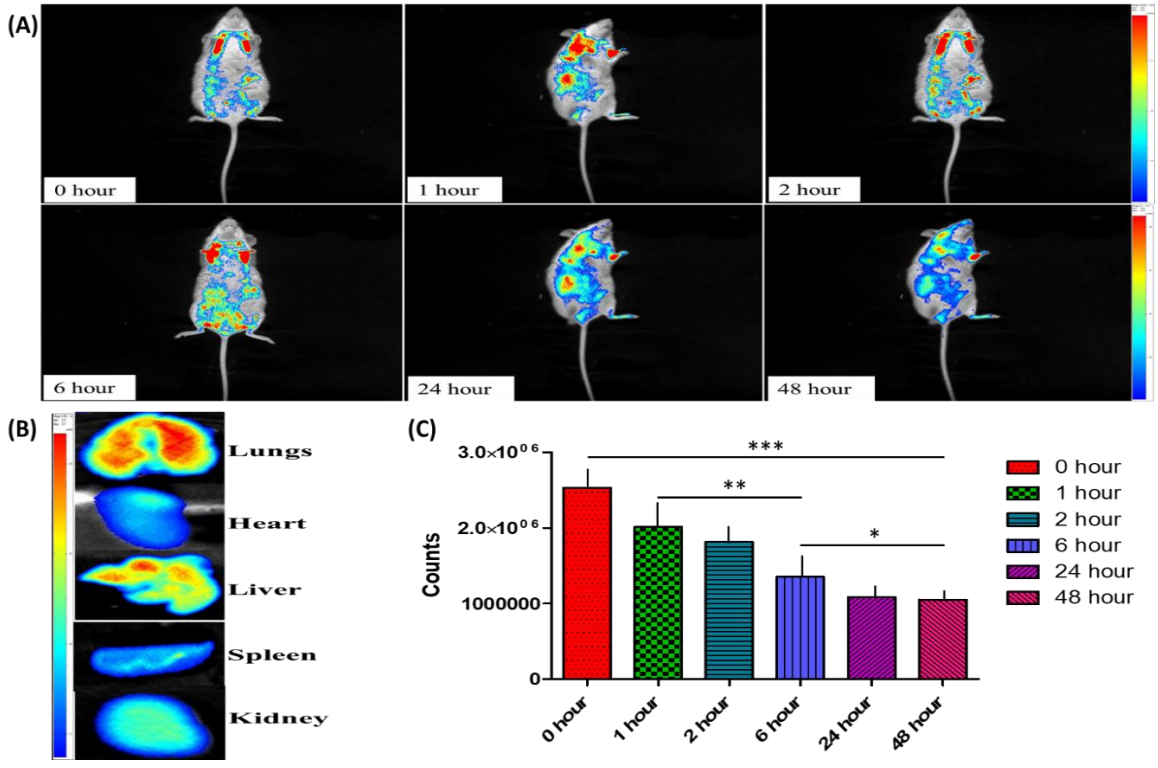

Figure 27: (A) IVIS images of mice after intranasal instillation of GEM-EGCG SLNs at different time points, depicting qualitative biodistribution of GEM-EGCG SLNs in the body; (B) IVIS images depicting biodistribution of GEM-EGCG SLNs in the vital organs after 48 hours; (C) Graph representing ROI (region of interest) quantification in terms of

bioluminescence signals of GEM-EGCG SLNs by IVIS imaging system in the lungs of mice at different time points, (the data has been presented as mean ± SD (n=3) and statistical values represent ($*p < 0.05$), ($**p < 0.01$), ($***p < 0.001$) are statistically significant and ($p > 0.05$) non-significant (ns)).

5.8 Biodistribution study

Biodistribution studies were performed in female Wistar rats, 250 g ± 10 g, after 1 hour and 6 hours of intranasal administration to evaluate the targeting efficiency. The biodistribution results (figure 28) show that within 1 hour of intranasal administration, both GEM and EGCG showed random distribution to the liver. Pure GEM and pure EGCG had higher biodistribution in the liver compared to their SLNs forms, including GEM-EGCG SLNs, GEM SLNs, and EGCG SLNs. The lower biodistribution of GEM and EGCG in their SLNs forms is attributed to the sustained release provided by the SLNs. This controlled release mechanism slows down the rate at which the drugs are distributed throughout the body. In contrast, pure GEM and pure EGCG are free from the encapsulation matrix of SLNs. As a result, they are distributed more quickly and widely across the body, leading to higher concentrations in the liver shortly after administration.

The findings suggest that while pure drugs are rapidly distributed, the use of SLNs for drug delivery offers a controlled and sustained release. This can be beneficial for reducing systemic side effects and ensuring that the drug remains at the target site for a longer duration, enhancing therapeutic efficacy. This data underscores the potential of SLNs as an effective delivery system for targeted therapies, particularly in conditions like cancer where maintaining a consistent drug concentration at the target site is crucial.

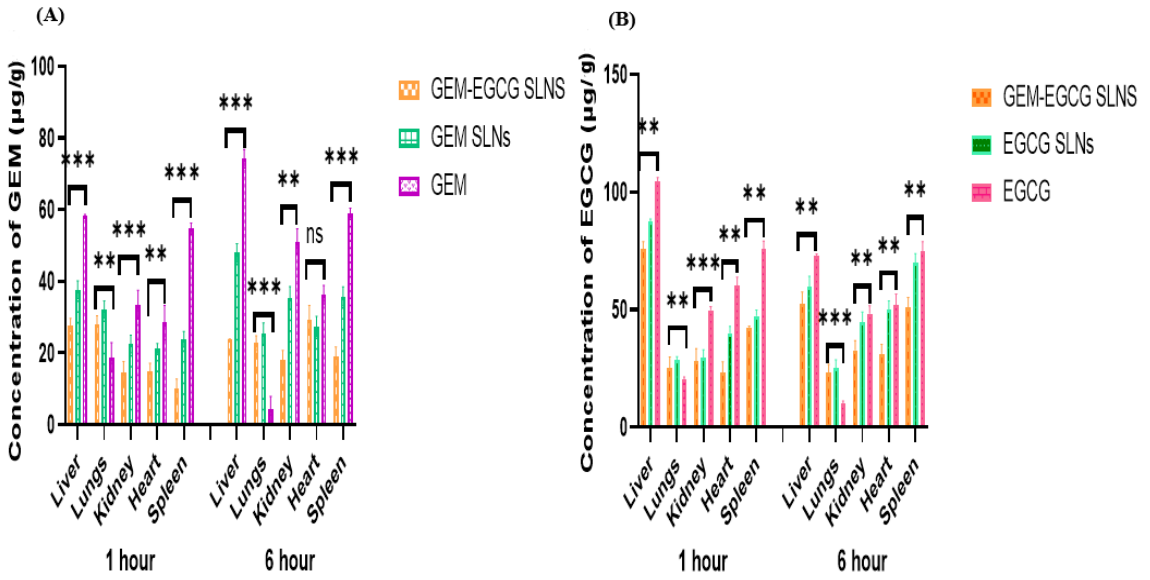

Figure 28: Bar diagram representation of relative biodistribution of GEM and EGCG in the vital organs after 1 hour and 6 hours of intranasal instillation of GEM-EGCG SLNs, EGCG SLNs, GEM SLNs, GEM, and EGCG (the data has been presented as mean ± SD (n=3) and statistical values represents *** ($p < 0.001$), ** ($p < 0.01$), and ns (non-significant)) (abbreviations: GEM- gemcitabine; EGCG- epigallocatechin-3-gallate; GEM-EGCG SLNs- gemcitabine and epigallocatechin-3-gallate loaded solid lipid nanoparticles; GEM SLNs- gemcitabine loaded solid lipid nanoparticles; EGCG SLNs- epigallocatechin-3-gallate loaded solid lipid nanoparticles)

In comparison to the lungs, kidney, heart, and spleen, both drugs were found to be highly biodistributed in the liver, which could be reasoned as the liver is the main metabolizing organ for GEM and EGCG. Pure GEM was found to be present in high concentrations post 1 and 6 hours in the liver, whereas GEM-EGCG SLNs and GEM SLNs have shown a fall-off in the biodistribution of GEM in the liver. A similar pattern was observed for the biodistribution of EGCG from GEM-EGCG SLNs and EGCG SLNs in comparison to pure EGCG. The highest concentration was found to be present in the liver, kidney, and spleen which could be accredited to the fact that these are the major organs responsible for the metabolism of GEM

[207] and EGCG [208] but it is comprehensible from figure 28 that the concentration of GEM and EGCG present in these major organs responsible for metabolism is less in case of GEM-EGCG SLNs, GEM SLNs, and EGCG SLNs as compared to pure GEM and pure EGCG, which signifies the protective effect of SLNs against biodistribution and hence clearance of drugs from the body [209]. The other possible justification for greater biodistribution of SLNs to the liver and spleen is rapid uptake by the reticuloendothelial system by the mechanism of endocytosis and phagocytosis. Lipidic systems are actively taken up by organs of the reticuloendothelial system [210], [211], [212]. The slow and sustained release of GEM and EGCG from SLNs hinders the process of biodistribution for GEM and EGCG and more amount of the drug is present at the desired site which is the lungs in the present study. SLNs are present in greater concentration in lungs as compared to pure GEM and pure EGCG because of the EPR effect of tumor cells which allows greater penetration of nanosized SLNs into lung tumor cells owing to their leaky vasculature and reduced drainage by the lymphatic system[213], [214].

5.9 Histopathological study

Histological sections of mice represent adenocarcinoma-type lesions characterized by nests of cells corresponding to perforations kind of sieves as presented in figure 29 (A). Moderate atypical adenomatous hyperplasia [215] in the bronchioles was observed in the histological sections from this group along with the thickening of the epithelium corresponding to epithelial hyperplasia (atypical adenomatous hyperplasia is the proliferation of columnar epithelial cells or cuboidal epithelial cells of bronchioles and alveoli of the respiratory tract. The lesions of atypical adenomatous hyperplasia correspond to a size of < 5 millimeters in diameter and are often multiple [216]). Images from treatment group GEM-EGCG SLNs show very few pathological lesions which support the potential of anti-tumor efficacy of GEM-EGCG SLNs as presented in figure 29 (B).

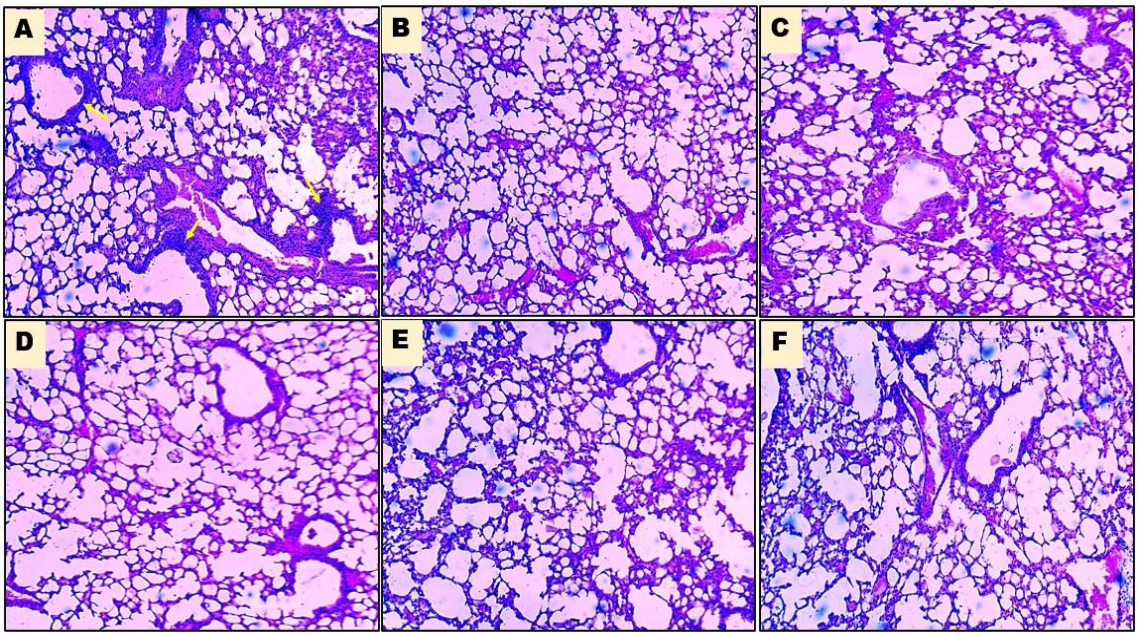

Figure 29: Histological images from the groups- (A) diseased control group; (B) GEM-EGCG SLNs treatment group; (C) GEM SLNs treatment group; (D) EGCG SLNs treatment group; (E) GEM drug control group; and (F) EGCG drug control group.

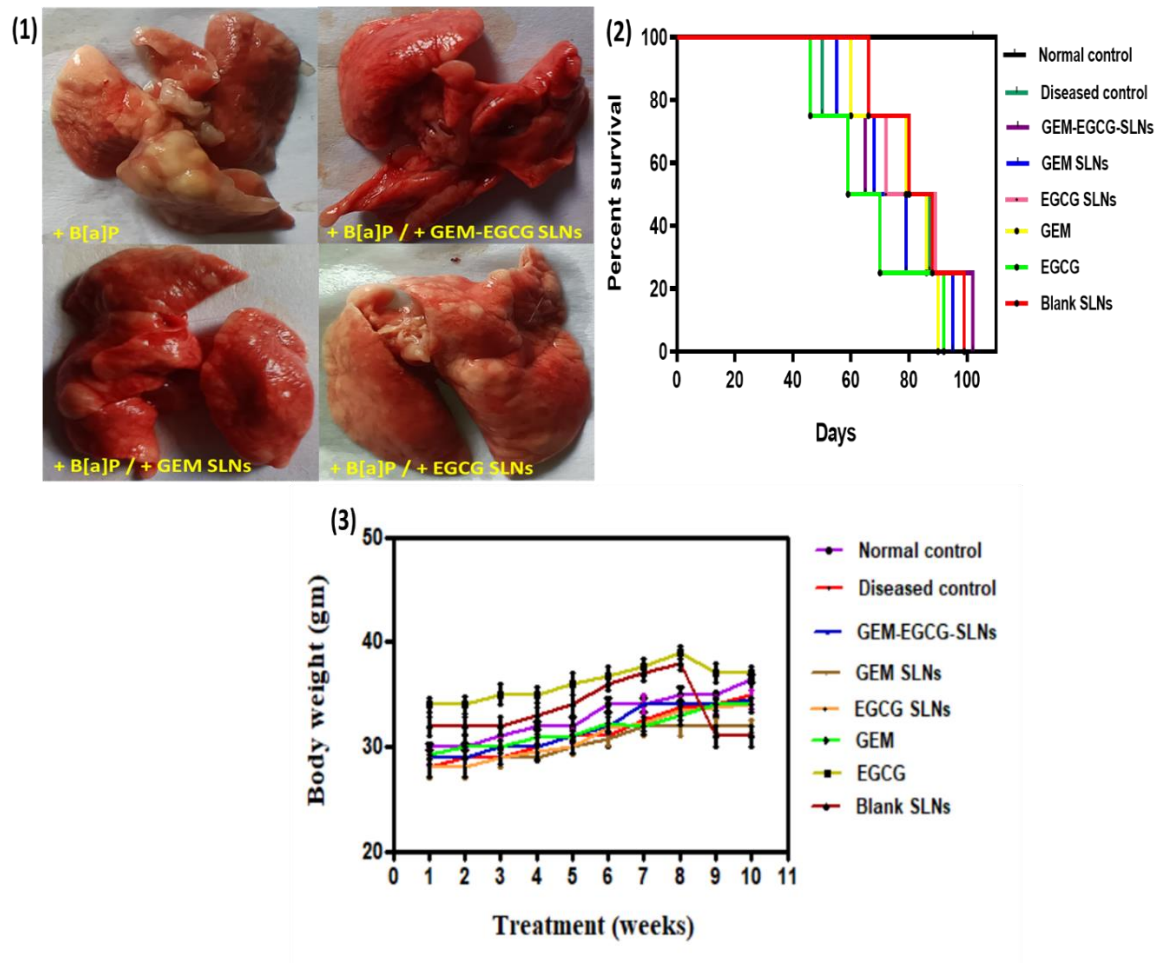

Figure 30: (1) Images of lungs excised from different treatment groups at the end of study (3 months); (2) Survival analysis curve- Kaplan Meier curve, depicting the survival of different treatment groups over 100 days; (3) Curve depicting body weight changes in subjects from different treatment groups over the treatment period (abbreviations: GEM- gemcitabine; EGCG- epigallocatechin-3-gallate; GEM-EGCG SLNs- gemcitabine and epigallocatechin-3-gallate loaded solid lipid nanoparticles; GEM SLNs- gemcitabine loaded solid lipid nanoparticles; EGCG SLNs- epigallocatechin-3-gallate loaded solid lipid nanoparticles; blank SLNs- blank solid lipid nanoparticles; B[a]P- benzopyrene; +B[a]P- receiving benzopyrene; +B[a]P/+GEM-EGCG SLNs- receiving benzopyrene and GEM-EGCG SLNs; +B[a]P/+GEM SLNs- receiving benzopyrene and GEM-SLNs; +B[a]P/+EGCG SLNs- receiving benzopyrene and EGCG SLNs).

Histological sections taken from the GEM drug control group and EGCG drug control group (figure 29 (E & F)), represent mild atypical adenomatous hyperplasia in the bronchioles and epithelial hyperplasia [217], [218]. Histological sections from GEM SLNs treated group and EGCG SLNs treated group (figure 29 (C & D)) represent regions of lesions with very slight atypical adenomatous hyperplasia contributing to the efficacy of monostearate-based SLNs as drug carrier and therapeutic potentials of GEM SLNs and EGCG SLNs when compared to GEM drug control and EGCG drug control group.

5.10Assessment of safety and biocompatibility of SLNs

5.10.1 Safety assessment of SLNs in the major metabolizing organs

Histopathological investigation of the major organs viz., liver, and kidney (figure 31) was performed to study any susceptibility of pathological lesions post intranasal administration of the saline (control group), and blank SLNs. The histological images from the control group and blank SLNs treated group confirm the safety of the monostearate-based SLNs carrier system as no pathological lesions were observed in the kidney and liver of the Swiss albino mice. Histological images of the kidney show clear glomerular cells and Bowman's capsule without any pathological lesions. The histological investigation postulates the safety of the formulation to be used in the study.

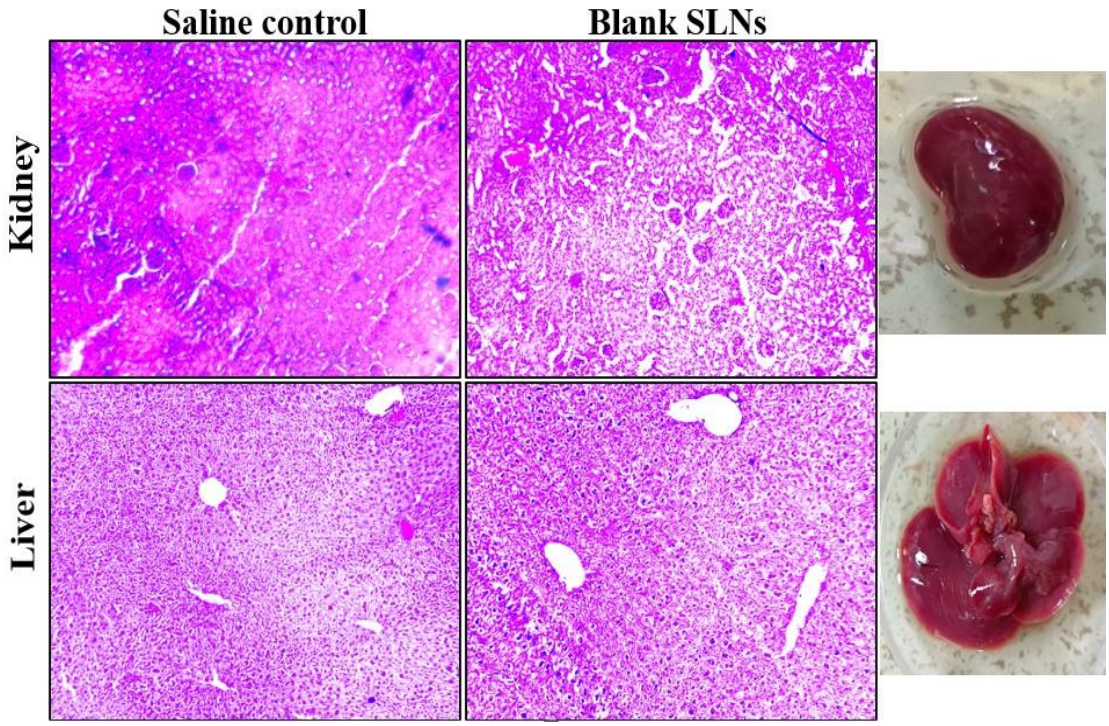

Figure 31: Histopathological images of the major metabolizing organs viz., kidney and liver to assess the safety of SLNs.

5.10.2 Safety assessment of SLNs in the blood-Hemolysis study

Biocompatibility of GEM-EGCG SLNs with blood was assessed by a hemolysis study. Chemotherapy is often associated with hemolysis due to an interaction between drug particles with the membrane of erythrocyte which results in the lysis of erythrocyte cells along with enzyme degradation and hydrolysis [163]. We observed a hemolysis rate of 1.62 ± 0.10 % for GEM-EGCG SLNs, 2.95 ± 0.21 % for GEM, and 1.66 ± 0.13 % for EGCG at a concentration of 125 µg/mL. Other dilutions of Gem-EGCG SLNs, GEM, and EGCG demonstrated very low values of hemolysis as represented in figure 32. The reduction in the rate of hemolysis for GEM-EGCG SLNs as compared to pure drug GEM and EGCG could be attributed to the presence of lipids and phospholipids in SLNs which provides a layer that acts as a shield on the surface and leads to attenuation of the hemolysis rate. Further, the drugs are present in the

inner matrix of SLNs which prevent the interaction of GEM and EGCG with the membrane of erythrocyte cells [76].

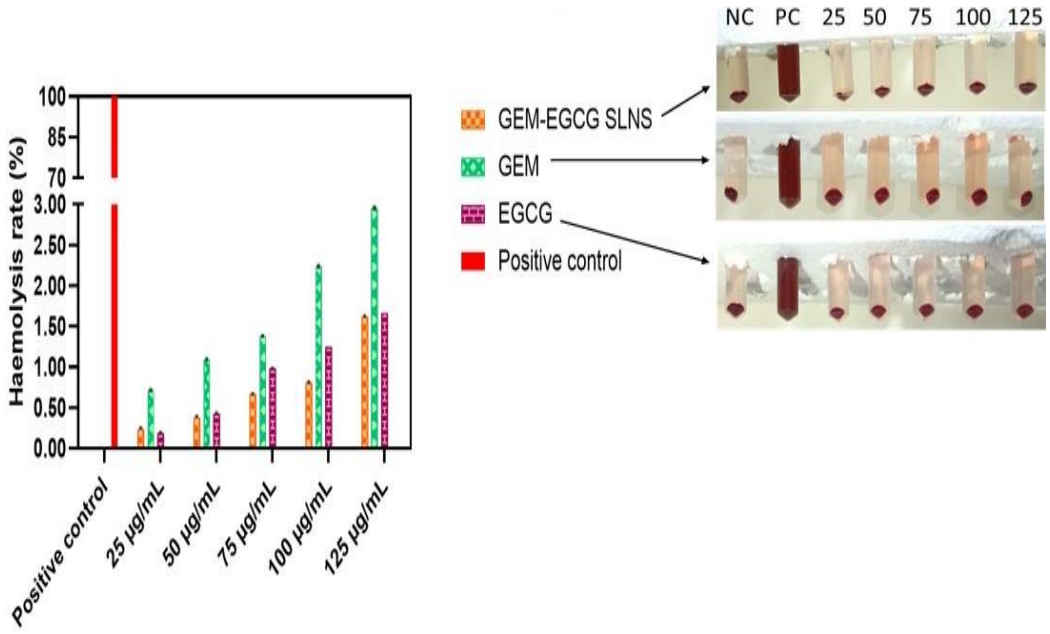

Figure 32: Bar graph representation of the hemolysis rate (%) at different concentrations of GEM-EGCG SLNs, GEM, EGCG, and positive control (triton X-100). The supporting photograph is from the experiment of the hemolysis study performed in different groups (NC: negative control; PC: positive control)(the data has been presented as mean ± SD (n=3)) (abbreviations: GEM- gemcitabine; EGCG- epigallocatechin-3-gallate; GEM-EGCG SLNs- gemcitabine and epigallocatechin-3-gallate loaded solid lipid nanoparticles; blank SLNs- blank solid lipid nanoparticles).

Based on the hemolysis study, histopathology, and biocompatibility studies wherein no pathological lesions and toxicity were observed in the eliminating organs, in the lungs, and blood, it can be suggested that the SLNs will be biocompatible with the nasal tissue. Moreover, the ingredients used (glyceryl monostearate, 1 % polyvinyl alcohol, 1 % pluronic F-127, and hydrogenated soy phosphatidylcholine) in the SLNs are ‘GRAS certified' and are

biocompatible and biodegradable. Further, the encapsulation of the drug in the SLNs does not directly expose the nasal tissue to the drug which might be toxic.

5.10.3 Safety assessment of GEM-EGCG SLNs in the nasal region of Swiss albino mice

Additionally, the design of the formulation allows only a small amount of drug release (if any) to occur at the nasal tissue because of the sustained release nature of the formulation. Moreover, following the intranasal administration of the formulation, we conducted a histological analysis of the nasal mucosa tissue (figure 33). The study findings revealed that the nasal mucosa of the treatment group appeared normal compared to the control group that received no treatment. The columnar goblet cells and basal cells of the nasal epithelium were visible and had no distortion in morphology or shape.

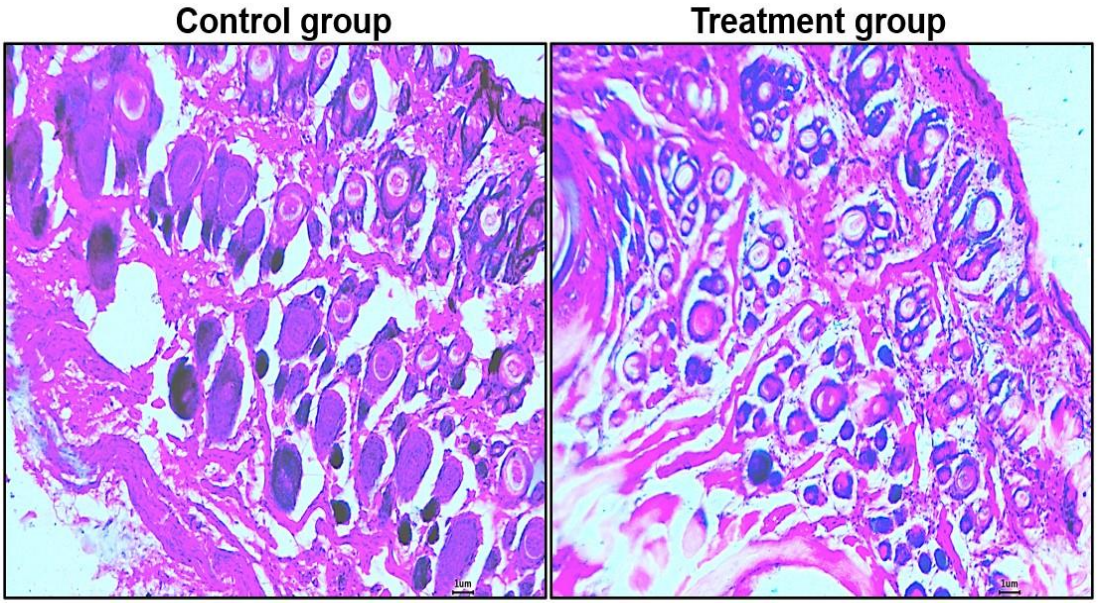

Figure 33: Histopathological images of the nose of mice after intranasal instillation of GEM-EGCG SLNs (treatment group) compared with control group.

Moreover, the lamina propria region of the treatment group appeared normal with no distortion or pathological lesions in its structure, as compared to the histology image of the

normal group [219], [220]. These results indicate that GEM-EGCG SLNs are safe for use in the nasal region of mice.